

Overconstrained estimates of neutrinoless double beta decay within the QRPA

A. Faessler,¹ G.L. Fogli,^{2,3} E. Lisi,³ V. Rodin,¹ A.M. Rotunno,^{2,3} and F. Šimkovic¹

¹ *Institute of Theoretical Physics, University of Tuebingen,
72076 Tuebingen, Germany*

² *Dipartimento Interateneo di Fisica “Michelangelo Merlin,”
Via Orabona 4, 70126 Bari, Italy*

³ *Istituto Nazionale di Fisica Nucleare, Sezione di Bari,
Via Orabona 4, 70126 Bari, Italy*

Estimates of nuclear matrix elements for neutrinoless double beta decay ($0\nu2\beta$) based on the quasiparticle random phase approximations (QRPA) are affected by theoretical uncertainties, which can be substantially reduced by fixing the unknown strength parameter g_{pp} of the residual particle-particle interaction through one experimental constraint — most notably through the two-neutrino double beta decay ($2\nu2\beta$) lifetime. However, it has been noted that the g_{pp} adjustment via $2\nu2\beta$ data may bring QRPA models in disagreement with independent data on electron capture (EC) and single beta decay (β^-) lifetimes. Actually, in three nuclei of interest for $0\nu2\beta$ decay (^{100}Mo , ^{116}Cd and ^{128}Te), for which all such data are available, we show that the disagreement vanishes, provided that the axial vector coupling g_A is treated as a free parameter, with allowance for $g_A < 1$ (“strong quenching”). Three independent lifetime data ($2\nu2\beta$, EC, β^-) are then accurately reproduced by means of two free parameters (g_{pp} , g_A), resulting in an overconstrained parameter space. In addition, the sign of the $2\nu2\beta$ matrix element $M^{2\nu}$ is unambiguously selected ($M^{2\nu} > 0$) by the combination of all data. We discuss quantitatively, in each of the three nuclei, these phenomenological constraints and their consequences for QRPA estimates of the $0\nu2\beta$ matrix elements and of their uncertainties. We also comment on further experimental and theoretical work which might shed light on the surprisingly strong quenching of g_A suggested by our phenomenological analysis.

PACS numbers: 23.40.-s, 23.40.Hc, 21.60.Jz, 27.60.+j

I. INTRODUCTION

The new paradigm of massive and mixed neutrinos, emerging from the recent evidence for neutrino flavor oscillations [1, 2, 3, 4], is still incomplete in several aspects. In particular, the nature of the neutrino fields (Dirac or Majorana) remains undetermined, the amount of CP violation in the neutrino sector (if any) is unconstrained, and the absolute neutrino masses—as well as their ordering—are not yet known. The process of neutrinoless double beta decay ($0\nu2\beta$),

$$(Z, A) \rightarrow (Z + 2, A) + 2e^- \quad (0\nu2\beta) , \quad (1)$$

bears on all these issues and, thus, is a major research topic in current experimental and theoretical neutrino physics [5, 6, 7, 8]. The claimed observation of $0\nu2\beta$ decay in ^{76}Ge with lifetime $T_{1/2}^{0\nu} \simeq 2.2 \times 10^{25}$ y [9], and the projects aimed at its independent (dis)confirmation [8], have also given new impetus to the field.

In general, barring contributions different from light Majorana neutrino exchange, the inverse $0\nu2\beta$ lifetime in a given nucleus is the product of three factors,

$$\left(T_{1/2}^{0\nu}\right)^{-1} = G^{0\nu} |M^{0\nu}|^2 m_{\beta\beta}^2 , \quad (2)$$

where $G^{0\nu}$ is a calculable phase space factor, $M^{0\nu}$ is the $0\nu2\beta$ nuclear matrix element, and $m_{\beta\beta}$ is the (nucleus-independent) “effective Majorana neutrino mass” which, in standard notation [10], reads

$$m_{\beta\beta} = \left| \sum_{i=1}^3 m_i U_{ei}^2 \right| , \quad (3)$$

m_i and U_{ei} being the neutrino masses and the ν_e mixing matrix elements, respectively.

The calculation of the matrix element $M^{0\nu}$ in Eq. (2) for a candidate $0\nu2\beta$ nucleus is notoriously difficult. It requires the detailed description of a second-order weak decay from a double-even “mother” nucleus (Z, A) to a double-even “daughter” nucleus ($Z + 2, A$) via virtual states (with any multipolarity J^π) of the so-called “intermediate” nucleus ($Z + 1, A$). The decay can proceed through both Fermi (F) and Gamow-Teller (GT) transitions, plus a small tensor (T) contribution,

$$M^{0\nu} = M_{\text{GT}}^{0\nu} + M_{\text{T}}^{0\nu} - \frac{M_{\text{F}}^{0\nu}}{g_A^2} , \quad (4)$$

and detailed nuclear models are required to estimate the separate components $M_X^{0\nu}$ ($X = F, GT, T$). In the above expression, g_A is the effective axial coupling in nuclear matter, not necessarily equal to its “bare” free-nucleon value $g_A \simeq 1.25$ [11].

Modern calculations of $0\nu2\beta$ matrix elements are usually performed within either the quasiparticle random phase approximation (QRPA) [12, 13] or the nuclear shell model (NSM) [14] and their variants, sometimes with large differences among the results. We remind that the QRPA basis of nuclear many-particle configurations, on which the residual particle-hole and particle-particle interaction is diagonalized to build the nuclear excitations, is limited to iterations of two-quasiparticle ones (reducing to the particle-hole configurations when the pairing interaction is switched off); for details, see, e.g. [5, 6]. The advantage of the QRPA as compared to the NSM is that one can include essentially unlimited sets of single-particle states, even those forming the continuum of the positive-energy ones within the continuum-QRPA [15].

Painstaking but steady progress in both the QRPA and the NSM approaches is gradually leading to a better understanding—and to a reduction—of the differences among their results [8]. However, even in the most refined approaches, the estimates of $M^{0\nu}$ remain affected by various uncertainties, whose reduction is of paramount importance for both theory and experiment. Indeed, uncertainties in $M^{0\nu}$ propagate to the extracted value of (or limit on) $m_{\beta\beta}$ via Eq. (2), and affect directly the design of $0\nu2\beta$ experiments (in particular the detector size and the choice of the nucleus) needed to reach a given target sensitivity to $m_{\beta\beta}$ [8]. Among the sources of uncertainties one can quote: (1) inherent approximations and simplifications of the theory; (2) existence of free or adjustable model parameters; (3) problematic description of the strong short-range repulsive interaction between nucleons; and (4) uncertainties in the value of g_A .

The latter problem arises from the significant reduction (“quenching”) of the strength observed in nuclear GT transitions (see, e.g., [16]), which still lacks a clear experimental quantification and theoretical understanding. Two possible physical origins of the quenching have been discussed, one due to the Δ -isobar admixture in the nuclear wave function [17] and another one due to the shift of the Gamow-Teller strength to higher excitation energies induced by short range tensor correlations [18]. In the absence of a better prescription, the effect of quenching (in either QRPA or NSM calculations) is often simply evaluated by replacing the bare value $g_A \simeq 1.25$ with an empirical, quenched value $g_A \simeq 1$ [19]. However, there is no *a priori* reason to exclude values $g_A \lesssim 1$, which have indeed sometimes been advocated, especially within the NSM approach [14, 20].

In this context, we present a novel approach towards data-driven constraints on $M^{0\nu}$ calculations, assuming the possibility of strong quenching ($g_A < 1$) within the QRPA. This unconventional hypothesis makes theory and data agree in a number of cases, where previous attempts have systematically failed. Therefore, we think that our approach may lead to a fruitful discussion and a fresh look at the whole problem of quenching, from both the theoretical and the experimental viewpoint. We stress, however, that we simply treat $g_A < 1$ as a phenomenological possibility in this work, without any attempt to elaborate theoretical interpretations of the g_A values emerging from the data analysis.

Our work is structured as follows. In Sec. II we discuss the experimental data which can be used to benchmark the QRPA model. We adopt a selected data set, including the measured lifetimes of two-neutrino double beta decay, electron capture, and single beta decay for three nuclei (^{100}Mo , ^{116}Cd , and ^{128}Te). In Sec. III we compare these data with the corresponding QRPA results, assuming standard quenching ($g_A = 1$) or no quenching ($g_A = 1.25$). We face then the well-known problem that the theory cannot match two or more data at the same time, for any given value of the so-called particle-particle strength parameter g_{pp} . In Sec. IV we show that this problem can be phenomenologically removed if strong quenching ($g_A < 1$) is allowed. In this case, the two parameters (g_{pp} , g_A) are overconstrained by three independent data in each of the three chosen nuclei, as shown in Sec. V. In Sec. VI we propagate the estimated (g_{pp} , g_A) uncertainties to the calculation of $0\nu2\beta$ matrix elements and lifetimes, with and without the effects of short-range repulsive interactions. Finally, we summarize our results and discuss future perspectives in Sec. VII.

II. EXPERIMENTAL BENCHMARKS

In order to reduce the theoretical uncertainties, any nuclear model used in $0\nu2\beta$ calculations should be benchmarked by as many weak-interaction data [21] as possible. Relevant weak processes are listed in Eqs. (5)–(11) below.

Two-neutrino double beta decay ($2\nu2\beta$),

$$(Z, A) \rightarrow (Z + 2, A) + 2e^- + 2\bar{\nu}_e \quad (2\nu2\beta) , \quad (5)$$

is a second-order weak process ($|\Delta Z| = 2$) which probes the same mother and daughter nuclei as $0\nu2\beta$ decay. It has been observed in several nuclei, thus providing a particularly important benchmark. Indeed, it was extensively demonstrated in [12] that the spread of QRPA calculations can be significantly reduced by constraining the nuclear model with the corresponding experimental $2\nu2\beta$ decay lifetime (see [22] for earlier attempts). The $2\nu2\beta$ data help to

TABLE I: Compilation of experimental references for nine nuclear systems (A) of interest in $0\nu 2\beta$ decay (“ Z ”, “ $Z+1$ ”, “ $Z+2$ ” denote “mother”, “intermediate”, “daughter” nuclei, respectively). The entries refer to $2\nu 2\beta$ decay data ($|\Delta Z| = 2$) as well as to processes probing the so-called first and second leg ($|\Delta Z| = 1$). For β^- data, only decays from $J^\pi = 1^+$ states are considered. For muon capture (μC), the data in [41] actually refer to natural isotopic mixture of the $Z+2$ nucleus. See also: [42, 43] for proposed EC measurements at $A = 76, 82, 100, 116$, and 128; [43] for proposed ($^3\text{He}, t$) measurements at $A = 76$ and preliminary ($d, ^2\text{He}$) data at $A = 76$ and 96; [44] for preliminary μC data at $A = 76, 82$, and 150.

Nuclei				$ \Delta Z = 2$	$ \Delta Z = 1$, first leg			$ \Delta Z = 1$, second leg		
A	Z	$Z+1$	$Z+2$	$2\nu 2\beta$	EC	($^3\text{He}, t$)	(p, n)	β^-	($d, ^2\text{He}$)	μC
76	Ge	As	Se	[32]			[38]			[41]
82	Se	Br	Kr	[32]			[38]			
96	Zr	Nb	Mo	[32]						[41]
100	Mo	Tc	Ru	[32]	[33, 34]	[37]		[36]		
116	Cd	In	Sn	[32]	[35]	[37]	[39]	[36]	[40]	[41]
128	Te	I	Xe	[32]	[36]		[38]	[36]		
130	Te	I	Xe	[32]			[38]			
136	Xe	Cs	Ba	[32]						[41]
150	Nd	Pm	Sm	[32]						[41]

fix an important free model parameter, namely, the strength g_{pp} of the residual particle-particle interaction [23, 24], and thus to “calibrate” the QRPA estimates of $M^{0\nu}$. Despite the fact that the $2\nu 2\beta$ decay process probes only a subset of the intermediate states relevant for $0\nu 2\beta$ decay (i.e., only those with $J^\pi = 1^+$, via GT transitions), it is just the 1^+ contribution to the total $0\nu 2\beta$ matrix element that reveals a pronounced sensitivity to g_{pp} , in contrast to the other multipole contributions [25]. This observation justifies the aforementioned fitting procedure employed in [12].

First-order weak processes ($|\Delta Z| = 1$) related to $0\nu 2\beta$ decay can probe, in usual jargon, either the “first leg” of the decay (from the mother nucleus to the intermediate one) or its “second leg” (from the intermediate nucleus to the daughter one). Relevant examples for the first leg include the electron capture (EC) from a bound state (e_b^-),

$$e_b^- + (Z+1, A) \rightarrow (Z, A) + \nu_e \quad (\text{EC}) , \quad (6)$$

and the charge-exchange reaction via ($^3\text{He}, t$),

$$^3\text{He} + (Z, A) \rightarrow (Z+1, A) + ^3\text{H} \quad (^3\text{He}, t) , \quad (7)$$

as well as via (p, n),

$$p + (Z, A) \rightarrow (Z+1, A) + n \quad (p, n) . \quad (8)$$

The second leg is instead probed by the β^- decay,

$$(Z+1, A) \rightarrow (Z+2, A) + e^- + \bar{\nu}_e \quad (\beta^-) , \quad (9)$$

by the charge-exchange ($d, ^2\text{He}$) reaction,

$$^2\text{H} + (Z+2, A) \rightarrow (Z+1, A) + ^2\text{He} \quad (d, ^2\text{He}) , \quad (10)$$

and by ordinary muon capture (μC),

$$\mu^- + (Z+2, A) \rightarrow (Z+1, A) + \nu_\mu \quad (\mu C) . \quad (11)$$

See also [26] for a recent discussion of these and other possible weak processes, including future (anti)neutrino-nucleus charged-current reactions at low energy [27]. Clearly, any of the above first-order weak processes could be used to set useful constraints on the nuclear model. Indeed, using β^- decay has been advocated as an alternative to $2\nu 2\beta$ decay for fixing the g_{pp} parameter in QRPA [28, 29, 30]; μC data might be similarly used in the near future [31]. However, one should be aware that these data are currently more sparse than for $2\nu 2\beta$ decay and, sometimes, have inherent problems or limitations, as discussed below.

Table I shows the current experimental status of the seven processes listed in Eqs. (5–11), for nine nuclei of interest for $0\nu 2\beta$ decay searches. Data on $2\nu 2\beta$ decay lifetimes exist for all these nuclei [32]. Lifetimes for EC and β^- decay

TABLE II: Experimental input. Half-life data (with 1σ experimental errors) for $2\nu 2\beta$, EC, and β^- decay in ^{100}Mo , ^{116}Cd , and ^{128}Te . All logarithms are in base 10.

Nucleus	$\log(T_{1/2}^{2\nu}/y) \pm \sigma_{\text{exp}}$	Ref.	$\log ft(\text{EC}) \pm \sigma_{\text{exp}}$	Ref.	$\log ft(\beta^-) \pm \sigma_{\text{expt}}$	Ref.
^{100}Mo	18.85 ± 0.03	[32]	$3.96^{+0.11}_{-0.09}$	[34]	4.60 ± 0.01	[36]
^{116}Cd	19.48 ± 0.03	[32]	$4.39^{+0.10}_{-0.15}$	[35]	4.662 ± 0.005	[36]
^{128}Te	24.40 ± 0.06	[32]	5.049 ± 0.007	[36]	6.06 ± 0.05	[36]

have been measured only in three cases, $A = 100, 116$ and 128 (with $J^\pi = 1^+$ states for the intermediate nucleus) [33, 34, 35, 36]. In one case ($A = 100$), the most recent EC datum [34] appears to be in conflict with the older one [33]. Data on scattering processes are also sparse. Available μC data [41] are not particularly constraining, since they refer to the natural isotopic mixture containing the daughter nucleus; see however [45] for a comparison of QRPA calculations with μC data, and [44] for preliminary μC data in unmixed $A = 76, 82$, and 150 daughter nuclei. Charge-exchange reactions involve analyses of spectral data which are, in general, more difficult to be interpreted and modeled than decay lifetimes [46, 47]. Data for $(^3\text{He}, t)$ exchange are available only for $A = 100$ and 116 [37]. In the latter case, the measured GT strength is in conflict with the one derived from EC [35]. Data for $(d, ^2\text{He})$ exchange and $A = 116$ are reported in [40], where the GT strength distribution is, however, normalized to the reference β^- one [36] at small excitation energy, and thus it does not provide an entirely independent constraint. The (p, n) reaction has been instead studied in several nuclei [38, 39], with emphasis on the GT strength distribution (rather than on its normalization). For $A = 116$, it should be noted that the recent (p, n) data in [39] disagree with the $(^3\text{He}, t)$ data in [37], and are only in rough agreement with the EC data in [35].

Clearly, new and dedicated measurements are needed, both to solve the mentioned experimental discrepancies and to fill the missing entries in Tab. I [26, 42, 43]. In the meantime, one needs to select a (hopefully consistent) data set, in order to perform a meaningful comparison with theoretical calculations.

In this work we adopt the following approach: we ignore data from scattering processes (which would require spectral analyses) and we choose only those data which involve half-life measurements, namely, $2\nu 2\beta$, EC, and β^- decay. Our investigation is then restricted to the three nuclear systems for which all such data exist, namely, $A = 100, 116$, and 128 , which we shall often denote by the name of the “mother” nucleus (^{100}Mo , ^{116}Cd , and ^{128}Te , respectively). For $A = 100$, we discard the old EC datum, $\log ft(\text{EC}) \simeq 4.45$ [33], in favor of the new (albeit unpublished) one [34]. Table II shows the corresponding input data that will be used in our analysis, in terms of $\log T/y$ (for $0\nu 2\beta$) and of $\log ft$ (for EC and β^-), where f is the usual nuclear Fermi function. (Throughout this paper, $\log \equiv \log_{10}$.)

III. DATA VERSUS THEORY WITH STANDARD OR NO QUENCHING ($1 \leq g_A \leq 1.25$)

In the context of the QRPA, it has been convincingly shown in [12] that the spread of theoretical calculations can be significantly reduced, in each of the nine nuclei in Tab. I, by fixing the g_{pp} parameter in such a way to reproduce the measured $2\nu 2\beta$ lifetimes.¹ This approach has however been questioned in [28, 29], since the fitted value of g_{pp} appears to underestimate (overestimate) the EC (β^-) lifetime by a large factor, as compared with available experimental data. The alternative choice of fitting g_{pp} by reproducing, e.g., the β^- decay lifetime [29, 30], merely shifts the problem to other data (e.g., to the $2\nu 2\beta$ or EC lifetimes) which are no longer correctly reproduced; see also [48] for early examples of such a conflict. It is worth noticing that, in the related literature [12, 13, 30], g_A has been taking in the range $1 \lesssim g_A \lesssim 1.25$, i.e., between standard quenching ($g_A \simeq 1$) and no quenching ($g_A \simeq 1.25$). Within such range, the problem of fitting two or more data [among the three ($2\nu 2\beta$, EC, β^-) lifetimes] appears to be basically unsolved in the QRPA approach. Before discussing in the detail this problem in Secs. III A–III C below, we recall a few essential features of the QRPA.

The ($2\nu 2\beta$, EC, β^-) processes occur through GT transitions, either at first order in g_A (for EC, β^-) or at second order in g_A (for $2\nu 2\beta$). Therefore, theoretical estimates of the associated (logarithmic) lifetimes need to be performed only for $g_A = 1$, and can then be scaled for $g_A \neq 1$ as:

$$\log(ft) \rightarrow \log(ft/g_A^2) \text{ for EC and } \beta^- , \quad (12)$$

$$\log(T_{1/2}^{2\nu}) \rightarrow \log(T_{1/2}^{2\nu}/g_A^4) \text{ for } 2\nu 2\beta . \quad (13)$$

¹ It is worth noticing that, in general, the effective values of both g_{pp} and g_A may change in different nuclei.

Within this work, QRPA calculations of the above lifetimes have been performed both in large basis (l.b., default choice) and in small basis (s.b.). The small basis consists of 13 single-particle levels (oscillator shells $N = 3$ and 4, plus the $f + h$ orbits from $N = 5$), while the large basis contains 21 levels for ^{100}Mo and ^{116}Cd (all states from shells $N = 1, \dots, 5$), and 23 levels for ^{128}Te ($N = 1, \dots, 5$ and i orbits from $N = 6$), in accordance with the choice of [12, 49]. The small set corresponds to $1\hbar\omega$ particle-hole excitations, and the large one to about $4\hbar\omega$ excitations.

An important output of QRPA calculations is the $2\nu 2\beta$ matrix element $M^{2\nu}$, whose modulus is probed by the observable $T_{1/2}^{2\nu}$ according to

$$\frac{1}{T_{1/2}^{2\nu}} = G^{2\nu} \left(\frac{g_A}{1.25} \right)^4 |M^{2\nu}|^2, \quad (14)$$

where $G^{2\nu}$ is a calculable phase space factor, and the bare value of g_A (1.25) is explicitly factorized out to make contact with previous notation [12]. In QRPA calculations, $M^{2\nu}$ typically starts positive for $g_{pp} \ll 1$, then decreases and eventually changes sign as g_{pp} increases. The critical value g_{pp}^* where $M^{2\nu} = 0$ marks an infinite lifetime, $\log T_{1/2}^{2\nu} \rightarrow \infty$. It turns out that $\log ft(\text{EC})$ is continuous across g_{pp}^* , while $\log ft(\beta^-)$ diverges locally. For g_{pp} increasing slightly beyond this critical point, the calculated energy of the first excited state E_1 decreases and eventually vanishes, inducing a breakdown (the so-called “collapse”) of the QRPA solution. QRPA calculations become thus less reliable in the vicinity of the critical and collapse points.

Figure 1 shows the matrix element $M^{2\nu}$ as a function of g_{pp} for each of the three reference nuclei, in large basis. Similar results are found for small basis (not shown). In each panel, a vertical dotted line marks the critical value g_{pp}^* where $M^{2\nu}$ flips its sign. The value of $M^{2\nu}$ drops rapidly for $g_{pp} > g_{pp}^*$, and the QRPA collapse is eventually reached. Both positive and negative values of $M^{2\nu}$ may be phenomenologically acceptable in principle, although theoretical arguments suggest that $M^{2\nu} > 0$ [12]. Determining the sign of $M^{2\nu}$ is thus a relevant check of the theory.

The QRPA estimates of $M^{2\nu}$, as well as those of the $2\nu 2\beta$, EC, and β^- lifetimes, are affected by various sources of uncertainties. In Sec. V we shall deal with the uncertainties related to the (*a priori* unknown) values of g_{pp} and g_A , and to the size of the basis. However, even if g_{pp} and g_A were perfectly known and the basis size were irrelevant, the approximation inherent to the QRPA approach would introduce further theoretical errors on each estimated lifetime. The assessment of these errors is obviously difficult and, to some extent, even arbitrary—but it is necessary to gauge the (dis)agreement between theoretical estimates and data. Our educated guess for the *extra* theoretical uncertainties (besides those related to g_{pp} , to g_A , and to the basis size) is $\sim 20\%$ for both the EC and $2\nu 2\beta$ lifetimes, and $\sim 40\%$ for the β^- lifetime. In the latter case, a larger *relative* error is assumed, due to the smaller (by a factor 2–3) calculated values of the corresponding matrix element as compared with the ones for the EC. Accordingly, we attach the following ($\pm 1\sigma$) theoretical errors σ_{th} to each logarithmic lifetime, for any fixed values of (g_{pp}, g_A) in any basis:

$$\log(T_{1/2}^{2\nu}/y) : \quad \sigma_{\text{th}} = \pm 0.08, \quad (15)$$

$$\log ft(\text{EC}) : \quad \sigma_{\text{th}} = \pm 0.08, \quad (16)$$

$$\log ft(\beta^-) : \quad \sigma_{\text{th}} = \pm 0.15. \quad (17)$$

In the next three subsections we shall compare the data in Tab. II with the corresponding QRPA estimates for $g_A = 1$. It will be shown that, in none of the three reference nuclei, the QRPA results can be really made consistent with more than one datum at a time, within the quoted experimental and theoretical uncertainties. Moreover, it will become evident that higher g_A values (e.g., $g_A = 1.25$) can only worsen the situation.

A. ^{100}Mo data versus QRPA ($g_A = 1$)

Figure 2 illustrates the comparison between ^{100}Mo data and theoretical predictions for standard quenching ($g_A = 1$) in large basis, as a function of g_{pp} . The upper, middle, and lower panels refer to the $2\nu 2\beta$, EC, and β^- logarithmic lifetimes, respectively. In each panel, the horizontal band represents the experimental datum at $\pm 1\sigma$ (as taken from Tab. II), while the curved band represents the QRPA results, with $\pm 1\sigma$ theoretical spread as in Eqs. (15–17). Vertical dotted lines mark the critical value g_{pp}^* which separate the left, positive branch ($M^{2\nu} > 0$) from the right, negative branch ($M^{2\nu} < 0$). The preferred g_{pp} ranges—where the experimental and theoretical bands cross each other—appear to be quite different in the three panels of Fig. 2. In particular, there is no overlap between the preferred g_{pp} ranges in the upper and middle (or lower) panel, while there is only a marginal overlap between those in the middle and lower panels. Agreement between data and theory is never reached for all the three observables at the same time.

If one chooses the $2\nu 2\beta$ lifetime to fix g_{pp} (as advocated in [12]), then two preferred ranges are selected, one in the positive branch (around $g_{pp} \simeq 0.78$), and the other in the negative branch (around $g_{pp} \simeq 0.79$); see the upper panel

of Fig. 2. Although both ranges are phenomenologically viable, the one in the positive branch is usually adopted on theoretical grounds [12]. However, for $g_{pp} \simeq 0.78$, the theoretical EC (β^-) lifetime turns out to be significantly smaller (larger) than the experimental value. Similar problems occur for $g_{pp} \simeq 0.79$ in the negative branch.

Alternatively, one might use the β^- lifetime to fix g_{pp} (as advocated in [29, 30]). In this case, as evident from Fig. 2, one could get marginal agreement between both β^- and EC observables around $g_{pp} \simeq 0.75$, but only at the price of underestimating the measured $2\nu 2\beta$ lifetime by a factor of ~ 4 . With one choice or another, it seems that current QRPA calculations fail to reproduce all the three independent lifetimes at the same time.

The above discrepancies would become stronger by increasing the GT strength from its standard quenched value ($g_A \simeq 1$) to its bare value ($g_A \simeq 1.25$, not shown). For $g_A = 1.25$, according to Eqs. (12) and (13), the theoretical bands in Fig. 2 would be shifted downwards by $-4 \log g_A \simeq -0.4$ (upper panel) or by $-2 \log g_A \simeq -0.2$ (middle and lower panels). The preferred ranges of g_{pp} would then move to the right for $2\nu 2\beta$ and β^- , and to the left for EC, thus destroying even the marginal agreement existing between β^- and EC observables for $g_A = 1$. We conclude that, within the range $1 \lesssim g_A \lesssim 1.25$, current QRPA calculations cannot reproduce the three lifetime data (nor, to some extent, any two among them) for any value of g_{pp} . These graphical results will be numerically confirmed in Sec. V.

B. ^{116}Cd data versus QRPA ($g_A = 1$)

Figure 3 is analogous to Fig. 2, but for ^{116}Cd . The situation is very similar to ^{100}Mo , and the same qualitative considerations apply, although the preferred ranges of g_{pp} are different. Also in this case, it is not possible to reconcile the QRPA estimates with the three independent lifetime data for any value of g_{pp} , at fixed $g_A = 1$. The discrepancy becomes worse for $g_A = 1.25$ (not shown).

C. ^{128}Te data versus QRPA ($g_A = 1$)

Figure 4 is analogous to Fig. 2, but for ^{128}Te . Here the situation is particularly bad, since the EC datum (middle panel) is not reproduced by the theory for any value of g_{pp} . For $g_A = 1.25$ (not shown), this discrepancy would be even worse, as the theoretical band would be shifted downwards. Even discarding completely the EC datum, the preferred ranges of g_{pp} in the upper panel ($2\nu 2\beta$) and lower panel (β^-) of Fig. 4 do not overlap, either in the positive or in the negative branch. Once again, there is an overall disagreement between QRPA results and data, the worse the higher g_A .

We remark that Figs. 2–4 refer to QRPA calculations in large basis. Very similar results are obtained—and the same comments apply—to calculations in small basis (not shown).

IV. DATA VERSUS THEORY WITH STRONG QUENCHING ($g_A < 1$)

In the previous Section, we have shown that the QRPA fails to reproduce the three ($2\nu 2\beta$, EC, β^-) lifetimes in each of the three reference nuclei (^{100}Mo , ^{116}Cd , ^{128}Te), as far as g_A is taken in the usual range, $1 \lesssim g_A \lesssim 1.25$. In particular, the discrepancy becomes worse as one moves towards the upper end of this range. Conversely, the discrepancy can be expected to become less severe (and hopefully vanish) for $g_A < 1$, corresponding to a “strong quenching” of the GT coupling.

Values of g_A lower than unity, although rather unconventional in the QRPA literature, are not uncommon in NSM calculations. The NSM, being an *ab initio* approach, does not depend on phenomenological parameters such as g_{pp} , but of course retains the dependence on the axial coupling g_A , with the associated quenching uncertainties. Although a quenched value $g_A \sim 1$ seems to roughly provide the correct normalization of the GT strength, strongly quenched values $g_A < 1$ may occasionally be needed to bring NSM calculations in agreement with data [14, 20]. It is fair to say that, in the NSM approach, one is not committed to a strict range for g_A (such as $1 \lesssim g_A \lesssim 1.25$): any value $g_A \sim O(1)$ is generally accepted, if the data require so.

In both the QRPA and the NSM approach, the origin and size of the GT quenching remains in part obscure and uncertain from a theoretical viewpoint, and the inferred values of g_A fluctuate considerably in different data analyses, processes, and nuclei. Even for a fixed process and nucleus, it is not excluded that the quenching may be energy-dependent [45]. Therefore, the common practice of adopting either the standard quenched value $g_A \simeq 1$ or the bare value $g_A \simeq 1.25$ may be unnecessarily restrictive. It is perhaps more sensible to treat g_A as a free parameter of order unity, whose precise value needs to be constrained by the data themselves, rather than pre-assigned by theory—just as one does for g_{pp} . In the following, we thus adopt a purely phenomenological viewpoint, and show that specific

choices of g_A below unity (which will be more precisely derived in Sec. V) can bring QRPA calculations in agreement with all the three lifetime data in each of three reference nuclei.

A. ^{100}Mo data versus QRPA ($g_A = 0.74$)

Figure 5 is analogous to Fig. 2, but for the strongly quenched value $g_A = 0.74$. We anticipate that this value provides the best overall agreement of QRPA calculations (curved bands) with the data (horizontal bands). Around $g_{pp} \simeq 0.73$, all bands cross each other in the three panels. No such common crossing occurs in the negative branch, as also confirmed by numerical explorations. Besides selecting the positive branch, the data appear to prefer a particle-particle strength ($g_{pp} \simeq 0.73$) sufficiently far from the critical and collapse values, where the QRPA estimates become less reliable. The β^- theoretical band in the lower panel is rather steep around $g_{pp} \simeq 0.73$, and can thus provide, together with the experimental datum, both an upper and a lower bound to g_{pp} ; the upper (lower) bound can also be enforced by the $2\nu 2\beta$ (EC) observable, as evident in the upper (middle) panel. In perspective, a reduction of the EC error in the middle panel would be beneficial to better probe this strong-quenching scenario.

B. ^{116}Cd data versus QRPA ($g_A = 0.84$)

Figure 6 is analogous to Fig. 3, but for the strongly quenched value $g_A = 0.84$. A good overall agreement between theory and data is reached in a broad range $g_{pp} \simeq 0.4\text{--}0.6$. It is interesting to note that this range could be significantly restricted if the experimental errors of the EC datum [35] in the middle panel were reduced by a factor of two or more. Also in this case, the data unambiguously select the positive branch, and keep g_{pp} far from the critical and collapse points.

C. ^{128}Te data versus QRPA ($g_A = 0.39$)

Figure 7 is analogous to Fig. 4, but for the very strongly quenched value $g_A = 0.39$. Such a reduction of g_A is mainly driven by the EC datum: an upward shift as large as $-2 \log g_A \simeq 0.8$ is needed to bring the “low” theoretical curve (middle panel of Fig. 4) in agreement with the horizontal band (as realized in the middle panel of Fig. 7). In this case, theory and data also agree in the upper and lower panels of Fig. 7, within the broad range $g_{pp} \simeq 0\text{--}0.3$. Reduction of the experimental error in the upper panel ($2\nu 2\beta$) would clearly be helpful to reduce this range. Once again, the data unambiguously select the positive branch, and keep g_{pp} far from the critical and collapse points.

We remark that Figs. 5–7 refer to QRPA calculations in large basis. Very similar results are obtained—and the same comments apply—to calculations in small basis (not shown).

D. Discussion

Strong quenching ($g_A < 1$) appears to provide a phenomenological solution to the well-known overall discrepancy between QRPA results and lifetime data. This solution is nontrivial because: (1) two free parameters enable to reproduce very well, within 1σ uncertainties, three independent data (in each of three different nuclei); (2) the positive branch ($M^{2\nu} > 0$), which is favored by theoretical arguments, is unambiguously selected by the data; (3) the preferred values of g_{pp} are far enough from the critical and collapse values. Such data-driven features seem to be more than accidental facts, and suggest that $g_A < 1$ might be a realistic option within the QRPA. More accurate lifetime data (especially for EC and, to some extent, for $2\nu 2\beta$ decay), as well as further charge-exchange reaction data (not considered in this work) should provide additional probes of the strong quenching solution.

This solution is admittedly unconventional in the context of QRPA, where g_A has been customarily taken within the range $1 \lesssim g_A \lesssim 1.25$. In particular, a GT coupling as small as $g_A \simeq 0.4$ (for ^{128}Te) corresponds to an order-of-magnitude quenching $[(0.4/1.25)^2 \simeq 10^{-1}]$ which, although not unknown in the NSM literature, is hardly justifiable within the QRPA. It may be that in ^{128}Te (and, partly, also in ^{100}Mo and ^{116}Cd) strong quenching is associated to other effects (e.g., nuclear deformation [50, 51, 52], not considered in this work), whose degrees of freedom might be traded for milder variations of g_A . However, if new free parameters are added to g_{pp} and g_A , the data set must also be enlarged to provide meaningful and nontrivial constraints—not much would be learned, in general, by fitting N data with $\geq N$ parameters.

For the sake of simplicity, in this work we do not explore more elaborated scenarios with additional data and further QRPA degrees of freedom. We just take for granted the indication in favor of $g_A < 1$, and perform quantitative fits

to three selected data (the $2\nu 2\beta$, EC, and β^- lifetimes) via two parameters (g_{pp} , g_A). We shall thus obtain an overconstrained parameter space, used for subsequent $0\nu 2\beta$ calculations in Sec. VI. Despite the above caveats, this approach represents a step forward with respect to previous attempts, which aimed at reducing the $0\nu 2\beta$ model uncertainties in QRPA by fitting a single datum (either $2\nu 2\beta$ or β^-) through a single parameter (g_{pp}) at fixed g_A .

V. OVERCONSTRAINING THE (g_{pp} , g_A) PARAMETERS

We perform a least-square fit to the three data $x_1 = \log(T_{1/2}^{2\nu}/y)$, $x_2 = \log ft(\text{EC})$, and $x_3 = \log ft(\beta^-)$ in terms of the two free parameters (g_{pp} , g_A). The χ^2 function to be minimized is defined as

$$\chi^2(g_{pp}, g_A) = \sum_{i=1}^3 \frac{[x_i^{\text{exp}} - x_i^{\text{th}}(g_{pp}, g_A)]^2}{(\sigma_{\text{exp}}^i)^2 + (\sigma_{\text{th}}^i)^2}. \quad (18)$$

where all the ingredients have been defined in the previous Sections. Asymmetric experimental errors (see Tab. II) are properly included by choosing either the upper or lower error, according to the sign of the difference $x_i^{\text{th}} - x_i^{\text{exp}}$. The minimum search is performed by numerical scan over a dense grid in the (g_{pp} , g_A) rectangle $[0, 1] \otimes [0, 1.25]$. Given three data and two parameters, one expects $\chi_{\min}^2 \sim O(1)$ for a proper fit. The expansion around the best-fit values of (g_{pp} , g_A) at $\Delta\chi^2 = \chi^2 - \chi_{\min}^2 = n^2$ provides then the $n\sigma$ contours for such parameters [10]. In the following, we show the main results both in graphical and tabular form.

Figure 8 shows the results of the (g_{pp} , g_A) fit in large basis. In each of the three panels (corresponding, from top to bottom, to ^{100}Mo , ^{116}Cd , and ^{128}Te) a dot marks the best-fit point, surrounded by the 1, 2 and 3σ contours. Vertical dotted lines separate the positive and negative branches of $M^{2\nu}$. In all panels, the allowed regions are fully contained in the positive branch, thus confirming quantitatively the theoretical arguments in favor of $M^{2\nu} > 0$ [12]. The best-fit points are safely far from extremal values of g_{pp} (0 and $\sim g_{pp}^*$), but the allowed regions may extend towards one of them. In particular, the allowed range of g_{pp} is somewhat squeezed towards the critical value for ^{100}Mo , while it extends towards zero for ^{128}Te (and, at 3σ , also for ^{116}Cd). More accurate experimental data (especially from EC and, to some extent, from $2\nu 2\beta$ decay) would be helpful to shrink such ranges, as discussed in Sec. IV, and might thus prevent the occurrence of nearly extremal values of g_{pp} . Concerning g_A , strong quenching ($g_A < 1$) is definitely preferred at $> 3\sigma$ in all cases, and appears to be especially severe in ^{128}Te .

The numerical results of the (g_{pp} , g_A) fit in large basis are summarized in Table III. The fit quality is very good in all cases ($\chi_{\min}^2 \lesssim 1$) and the best-fit values for the three lifetimes are in striking agreement with the corresponding data in Tab. II, which are repeated for convenience in Table III (in square brackets). The best-fit values and $\pm n\sigma$ ranges ($n = 1, 2, 3$) for g_{pp} and g_A are also reported. (The g_A values adopted in Figs. 5–7 are just taken from Table III.)

We have repeated the analysis in small basis, with similar results. The graphical results are omitted, while the numerical ones are reported in Table IV. The quality of the fit is very good also in this case. The allowed ranges for g_{pp} and g_A in small basis (Tab. IV) are somewhat different from those in large basis (Table III), but with similar features. In particular, the allowed g_{pp} range is in the positive branch, and the general trend in favor of $g_A < 1$ is confirmed. We conclude that the main results obtained so far do not change qualitatively with the size of the basis.

TABLE III: Results of the (g_{pp} , g_A) fit for three different (mother) nuclei, with QRPA calculations performed in large basis. Column 2: minimum χ^2 . Columns 3–5: theoretical lifetimes for $2\nu 2\beta$, EC and β^- decay at best fit, to be compared with the experimental data in Tab. II which are repeated here in square brackets. Columns 6–9: value of g_{pp} at best fit, and allowed ranges at 1, 2 and 3σ . Columns 10–13: value of g_A at best fit, and allowed ranges at 1, 2 and 3σ .

Nuclei	χ_{\min}^2	$\log(T_{1/2}^{2\nu}/y)$	$\log ft(\text{EC})$	$\log ft(\beta^-)$	g_{pp}	$\pm 1\sigma$	$\pm 2\sigma$	$\pm 3\sigma$	g_A	$\pm 1\sigma$	$\pm 2\sigma$	$\pm 3\sigma$
^{100}Mo	1.26	18.82 [18.85]	4.09 [3.96]	4.66 [4.60]	0.733	+0.020 -0.020	+0.031 -0.063	+0.039 -0.126	0.741	+0.046 -0.037	+0.120 -0.074	+0.176 -0.107
^{116}Cd	0.12	19.49 [19.48]	4.35 [4.39]	4.63 [4.66]	0.493	+0.106 -0.149	+0.173 -0.358	+0.224 -0.493	0.843	+0.042 -0.037	+0.088 -0.075	+0.149 -0.106
^{128}Te	0.03	24.41 [24.40]	5.05 [5.05]	6.04 [6.06]	0.191	+0.126 -0.177	+0.216 -0.191	+0.283 -0.191	0.392	+0.023 -0.019	+0.046 -0.037	+0.074 -0.056

TABLE IV: As in Tab. III, but in small basis.

Nuclei	χ^2_{\min}	$\log(T_{1/2}^{2\nu}/y)$	$\log ft(\text{EC})$	$\log ft(\beta^-)$	g_{pp}	$\pm 1\sigma$	$\pm 2\sigma$	$\pm 3\sigma$	g_A	$\pm 1\sigma$	$\pm 2\sigma$	$\pm 3\sigma$
^{100}Mo	1.11	18.82 [18.85]	4.08 [3.96]	4.67 [4.60]	0.862	+0.024 -0.035	+0.043 -0.094	+0.055 -0.181	0.745	+0.042 -0.037	+0.098 -0.074	+0.172 -0.111
^{116}Cd	0.03	19.49 [19.48]	4.37 [4.39]	4.65 [4.66]	0.540	+0.130 -0.165	+0.220 -0.385	+0.283 -0.538	0.815	+0.042 -0.033	+0.084 -0.070	+0.139 -0.102
^{128}Te	0.01	24.40 [24.40]	5.05 [5.05]	6.05 [6.06]	0.198	+0.141 -0.189	+0.248 -0.198	+0.330 -0.198	0.397	+0.023 -0.019	+0.046 -0.037	+0.074 -0.056

VI. IMPLICATIONS FOR $0\nu 2\beta$ DECAY

In the previous Section we have obtained allowed regions in the parameter space (g_{pp}, g_A) . In this Section we study how such regions affect the QRPA calculation of $0\nu 2\beta$ decay, after recalling some basic features of this process.

The $(2\nu 2\beta, \text{EC}, \beta^-)$ processes that we have considered so far occur only via GT transitions through 1^+ intermediate states. The leading contribution $M_{\text{GT}}^{0\nu}$ to the amplitude of the neutrinoless double beta decay also comes from the GT-type transitions which, however, proceed through intermediate states of all, but 0^+ , multiplicities. In addition, there are Fermi $M_{\text{F}}^{0\nu}$ and (small) tensor $M_{\text{T}}^{0\nu}$ contributions to the $0\nu 2\beta$ matrix element,

$$M^{0\nu}(g_{pp}, g_A) = M_{\text{GT}}^{0\nu}(g_{pp}) + M_{\text{T}}^{0\nu}(g_{pp}) - \frac{M_{\text{F}}^{0\nu}(g_{pp})}{g_A^2}, \quad (19)$$

where the dependence on g_{pp} and g_A is made explicit.

Figure 9 shows the relevant components of the $0\nu 2\beta$ matrix elements as a function of g_{pp} in large basis, and including short range correlations, which will be shortly discussed below. Since their QRPA calculation is computer-intensive, g_{pp} is varied only within the relevant $\pm 3\sigma$ range shown in Fig. 8. Note that the leading component shows significant variations with g_{pp} , so that any constraint on this parameter (such as those derived in the previous Section) helps to reduce the spread of QRPA estimates of $0\nu 2\beta$ decay. Results qualitatively similar to Fig. 9 are obtained for small basis, or without short range correlations (not shown).

Given the QRPA results in Fig. 9, the $0\nu 2\beta$ matrix element can be computed for any relevant value of g_A and g_{pp} through Eq. (19). In order to make contact with the notation in [12], we shall actually rescale the matrix element as

$$M'^{0\nu} = M^{0\nu} \left(\frac{g_A}{1.25} \right)^2. \quad (20)$$

The $0\nu 2\beta$ lifetime reads then

$$T^{0\nu}(g_{pp}, g_A) = \frac{t_{1/2}^{0\nu}}{|M'^{0\nu}|^2}, \quad (21)$$

where the proportionality factor $t_{1/2}^{0\nu} = \left(m_{\beta\beta}^2 G^{0\nu} / 1.25^2 \right)^{-1}$ [y] is numerically given by

$$t_{1/2}^{0\nu} = \begin{cases} 1.83 \times 10^{27} & (^{100}\text{Mo}), \\ 1.68 \times 10^{27} & (^{116}\text{Cd}), \\ 4.74 \times 10^{28} & (^{128}\text{Te}), \end{cases} \quad (22)$$

for a reference Majorana mass $m_{\beta\beta} = 50$ meV. For different values of $m_{\beta\beta}$, one just rescales $t_{1/2}^{0\nu} \propto m_{\beta\beta}^{-2}$.

For any given value of (g_{pp}, g_A) , calculations of $M'^{0\nu}$ are affected not only by the size of the basis (either large or small), but also by uncertainties which are peculiar of the $0\nu 2\beta$ process, namely, those related to the important issue of short range correlations (s.r.c.). These correlations account for the well-known fact that the nucleon-nucleon interaction becomes strongly repulsive at small internucleon distances. This in turn must lead to strong suppression of the relative-motion wave function at small distances (s.r.c. effects). Short range correlations are explicitly included neither within the QRPA nor within the NSM. They are instead introduced ad hoc directly into the neutrino potential via a multiplicative factor (the square of a correlation function). One of the most popular is the Jastrow-like correlation function [53] which has been used in the previous calculations [12, 49] and is also used in this work. We shall thus present results in four cases, corresponding to either large or small basis, with or without the Jastrow-like s.r.c. effects.

TABLE V: QRPA estimates of the $0\nu 2\beta$ matrix elements $M'^{0\nu}$, including the effect of short range correlations. The central value and the allowed ranges of $M'^{0\nu}$ are derived, respectively, from the best-fit values and allowed ranges of (g_{pp}, g_A) . The estimates refer to both large basis (l.b.) and small basis (s.b.). We also report the corresponding (logarithmic) ranges for the $0\nu 2\beta$ lifetime $T_{1/2}^{0\nu}$ (in years), assuming a reference value $m_{\beta\beta} = 50$ meV.

Nucleus	$M'^{0\nu}_{\text{l.b.}}$	$\pm 1\sigma$	$\pm 2\sigma$	$\pm 3\sigma$	$M'^{0\nu}_{\text{s.b.}}$	$\pm 1\sigma$	$\pm 2\sigma$	$\pm 3\sigma$	$\log(T_{1/2}^{0\nu})_{\text{l.b.}}$	$\pm 1\sigma$	$\pm 2\sigma$	$\pm 3\sigma$	$\log(T_{1/2}^{0\nu})_{\text{s.b.}}$	$\pm 1\sigma$	$\pm 2\sigma$	$\pm 3\sigma$
^{100}Mo	2.66	+0.15 -0.14	+0.33 -0.25	+0.61 -0.35	2.45	+0.16 -0.15	+0.35 -0.25	+0.65 -0.34	26.411	+0.046 -0.046	+0.088 -0.100	+0.124 -0.180	26.485	+0.055 -0.055	+0.095 -0.116	+0.132 -0.204
^{116}Cd	2.44	+0.23 -0.18	+0.53 -0.32	+0.90 -0.44	2.15	+0.20 -0.16	+0.46 -0.29	+0.78 -0.41	26.448	+0.065 -0.079	+0.123 -0.169	+0.174 -0.272	26.561	+0.067 -0.079	+0.127 -0.169	+0.181 -0.271
^{128}Te	2.58	+0.25 -0.19	+0.38 -0.35	+0.48 -0.47	2.59	+0.27 -0.23	+0.40 -0.42	+0.49 -0.58	27.851	+0.068 -0.020	+0.126 -0.120	+0.173 -0.147	27.849	+0.080 -0.086	+0.153 -0.124	+0.222 -0.151

TABLE VI: As in Tab. V, but without short range correlations.

Nucleus	$M'^{0\nu}_{\text{l.b.}}$	$\pm 1\sigma$	$\pm 2\sigma$	$\pm 3\sigma$	$M'^{0\nu}_{\text{s.b.}}$	$\pm 1\sigma$	$\pm 2\sigma$	$\pm 3\sigma$	$\log(T_{1/2}^{0\nu})_{\text{l.b.}}$	$\pm 1\sigma$	$\pm 2\sigma$	$\pm 3\sigma$	$\log(T_{1/2}^{0\nu})_{\text{s.b.}}$	$\pm 1\sigma$	$\pm 2\sigma$	$\pm 3\sigma$
^{100}Mo	3.27	+0.16 -0.15	+0.34 -0.29	+0.63 -0.42	2.97	+0.17 -0.16	+0.36 -0.29	+0.67 -0.40	26.233	+0.041 -0.043	+0.080 -0.087	+0.117 -0.155	26.318	+0.048 -0.049	+0.089 -0.100	+0.125 -0.178
^{116}Cd	2.84	+0.25 -0.19	+0.57 -0.35	+0.98 -0.49	2.47	+0.22 -0.17	+0.49 -0.32	+0.84 -0.44	26.317	+0.061 -0.073	+0.116 -0.159	+0.165 -0.256	26.440	+0.063 -0.075	+0.119 -0.159	+0.171 -0.255
^{128}Te	2.99	+0.27 -0.21	+0.41 -0.36	+0.52 -0.49	2.99	+0.28 -0.24	+0.43 -0.44	+0.54 -0.61	27.725	+0.074 -0.062	+0.114 -0.112	+0.155 -0.139	27.724	+0.073 -0.079	+0.138 -0.116	+0.198 -0.142

In each of the four cases, the effect of the (g_{pp}, g_A) uncertainties on $M'^{0\nu}$ is estimated by marginalization [10], taking into account the fact that the same fixed value for the matrix element may be realized by different (“degenerate”) couples of values (g_{pp}, g_A) . More precisely, given the function $\chi^2(g_{pp}, g_A)$ defined in the previous Section, and for a fixed value $\tilde{M}'^{0\nu}$, we define a marginalized χ^2 function,

$$\chi^2(\tilde{M}'^{0\nu}) = \min_{\tilde{g}_{pp}, \tilde{g}_A} \chi^2(\tilde{g}_{pp}, \tilde{g}_A), \quad (23)$$

over the degenerate set of $(\tilde{g}_{pp}, \tilde{g}_A)$ obeying

$$M'^{0\nu}(\tilde{g}_{pp}, \tilde{g}_A) = \tilde{M}'^{0\nu}. \quad (24)$$

The minimization of $\chi^2(\tilde{M}'^{0\nu})$, and the expansion around the minimum at $\Delta\chi^2 = n^2$, provide the correct best-fit values and $n\sigma$ ranges for $M'^{0\nu}$, respectively. Since we are interested in $n \leq 3$, we perform a numerical marginalization over a dense, rectangular grid covering only the $\pm 3\sigma$ ranges of (g_{pp}, g_A) .

Tables V and VI provide an overview of the derived ranges for $M'^{0\nu}$ at 1, 2 and 3 σ (in large and small basis), with and without the effect of s.r.c., respectively. We also report the corresponding ranges for the measurable (log) lifetime $T_{1/2}^{0\nu}$, at the reference value $m_{\beta} = 50$ meV. Note the $\pm n\sigma$ ranges are generally asymmetric and do not scale linearly, in part as a consequence of the original one-sided g_{pp} limits at either 0 or $\sim g_{pp}^*$ (see Fig. 8). By comparing the results in Tables V and VI, it appears that the basis size is not the major source of systematic uncertainties. Conversely, the inclusion or exclusion of s.r.c. effects always induce changes $> 1\sigma$.

Figure 10 shows an overview of QRPA results for the nuclear matrix elements (including s.r.c. effects) in three different cases for each nucleus. From left to right, the first two cases correspond to the 1σ ranges from Table V, in large and small basis, respectively. The third case correspond to the results previously obtained in [12] for $g_A = 1$ (with correspondingly smaller error bars, due to the fixed g_A value). Remarkably, such results for $M'^{0\nu}$ [12] differ by $\lesssim 12\%$ from those obtained in this work, in spite of a marked difference in the central values of g_A and g_{pp} .

Summarizing, in each of the three nuclei examined it is possible: (i) to fit very well three data ($2\nu 2\beta$, EC, β^-) with two parameters (g_{pp}, g_A) , provided that $g_A < 1$; (ii) to exclude the negative branch $M^{2\nu} < 0$; and (iii) to derive robust ranges for $0\nu 2\beta$ observables. There remains a relative large uncertainty on the $0\nu 2\beta$ matrix element, associated with the size of short range correlation effects. Unfortunately, s.r.c. effects are peculiar of $0\nu 2\beta$ decay and are not constrained at all by the ($2\nu 2\beta$, EC, β^-) data considered in this work.

VII. CONCLUSIONS AND PERSPECTIVES

It was shown in [12] that, by fitting g_{pp} in order to reproduce in calculations the corresponding experimental $2\nu 2\beta$ decay lifetimes, the sensitivity of calculated $0\nu 2\beta$ matrix elements to other ingredients of the QRPA, such as the basis size, can be successfully removed. Also, it was shown that the sensitivities of the results to g_A gets much milder than one could naively expect. There are also different proposals for fixing g_{pp} , for instance, by reproducing the single beta decay observables as advocated in [28, 29]. By fitting g_{pp} to reproduce the β^- lifetimes of the ground states of the intermediate nucleus one gets the results which are similar to the ones obtained in [12], but the EC or $2\nu 2\beta$ lifetimes are not reproduced. In this paper we have tried to reconcile all these data (available for the three nuclei ^{100}Mo , ^{116}Cd , and ^{128}Te) by letting g_A to be a free parameter of the model. In each nucleus, we have then found systematic indications in favor of strong quenching ($g_A < 1$), and we have been able to overconstrain two parameters (g_{pp} , g_A) with three lifetime data ($2\nu 2\beta$, EC, β^-), as well as to fix the sign of $M^{2\nu}$ (> 0).

The quenching of g_A for ^{100}Mo and ^{116}Cd obtained in this work ($g_A \simeq 0.74$ and $g_A \simeq 0.84$, respectively), although unconventional, is not much stronger than the typical values obtained within the NSM for lighter nuclei [14]. In contrast, the very strong quenching $g_A \simeq 0.39$ for ^{128}Te seems more difficult to explain and probably calls for other (concurrent) effects. For instance, it might be partially due to neglect of nuclear deformation in the present work. Importance of this effect has been demonstrated in [51] for the case of the $2\nu 2\beta$ decay. The experimental value of the parameter of the quadrupole deformation $\beta = 0.18$ for ^{128}Xe [54] has been shown in [51] to agree well with the corresponding theoretical value of $\beta = 0.15$. The change in the deformation from an almost spherical ^{128}Te to a rather well deformed ^{128}Xe gives rise to a reduction of the $2\nu 2\beta$ transition probability, that might be simulated here by a very strongly quenched g_A . The analysis of this possibility, and of other effects which might relax the need for very strong quenching, is left to future work.

The physical origin of the quenching of g_A has been discussed in the past. One explanation [17] assigns this effect to the Δ -isobar admixture in the nuclear wave function. Another—more generally accepted—explanation [18] assigns the quenching to the shift of the Gamow-Teller strength to higher excitation energies due to the short range tensor correlations. In light nuclei the quenching found in M1 transitions reduces g_A from its bare value (~ 1.25) to the in-medium one (~ 1). But the actual quenching in nuclear structure calculations can depend as on the detailed nuclear environment as on the truncations inherent to the model such as, for example, the basis size. Therefore, it appears useful to revisit the theoretical explanations of quenching, in order to check if and how they can cover cases with $g_A < 1$, as those emerging from our phenomenological analysis.

From the experimental viewpoint, it has been already mentioned that future EC data [42, 43] will be especially relevant in improving the (g_{pp} , g_A) parameter constraints. Moreover, the strong quenching of the axial vector coupling constant g_A should be observed not only in single and double beta decays, but also in M1 transitions. Therefore, the study of charge-exchange reactions as (p, n) , (n, p) , $(^3\text{He}, t)$ and $(d, ^2\text{He})$ [20, 40, 47] can shed new light on this issue. It is imperative, however, that the data are analyzed with no prior or hidden hypotheses about the GT coupling g_A . In conclusion, we think that the results of this work offer a novel possibility to reconcile QRPA results with experimental data, which deserves further discussions and tests, and warrants a revisitation of the quenching problem from a new perspective.

Acknowledgments

This work is supported in part by the EU ILIAS project under the contract RII3-CT-2004-506222. The work of G.L.F., E.L., and A.M.R. is also supported by the Italian Istituto Nazionale di Fisica Nucleare (INFN) and Ministero dell'Università e Ricerca (MiUR) through the “Astroparticle Physics” research project. A.F., V.R., and F.Š. acknowledge support of the Transregio SFB Project TR27 “Neutrinos and Beyond” of the Deutsche Forschungsgemeinschaft; in addition, F.Š. was supported by the VEGA Grant agency of the Slovak Republic (contract No. 1/0249/03) and by the DFG (436 SLK 17/298).

E.L. thanks the Institute of Theoretical Physics (Tuebingen, Germany), where this work was initiated, for kind hospitality. Preliminary results of this work were presented by E.L. at the νMASS workshop (Genova, Italy, 2007), and by V.R. at the 4th ILIAS-IDEA annual meeting (Paris, France, 2007). We thank Petr Vogel for early discussions about global experimental constraints on QRPA models.

-
- [1] G.L. Fogli, E. Lisi, A. Marrone, and A. Palazzo, *Prog. Part. Nucl. Phys.* **57**, 742 (2006).
 - [2] M. Maltoni, T. Schwetz, M.A. Tórtola and J.W.F. Valle, *New J. Phys.* **6**, 122 (2004).
 - [3] M.C. Gonzalez-Garcia and M. Maltoni, arXiv:0704.1800 [hep-ph].
 - [4] A. Strumia and F. Vissani, arXiv:hep-ph/0606054.
 - [5] A. Faessler and F. Šimkovic, *J. Phys. G* **24**, 2139 (1998).
 - [6] J. Suhonen and O. Civitarese, *Phys. Rept.* **300**, 123 (1998).
 - [7] P. Vogel, Lecture notes at *TASI'06*, Theoretical Advanced Study Institute in Elementary Particle Physics (Boulder, CO, 2006), World scientific, to appear [arXiv:hep-ph/0611243]; talk at *NOW 2006*, Proceedings of the Neutrino Oscillation Workshop (Conca Specchiulla, Italy, 2006), ed. by P. Bernardini, G.L. Fogli, and E. Lisi, *Nucl. Phys. B* **168** (Proc. Suppl.), 23 (2007).
 - [8] F.T. Avignone III, S.R. Elliott, and J. Engel, arXiv:0708.1033 [nucl-ex], submitted to *Rev. Mod. Phys.*
 - [9] H.V. Klapdor-Kleingrothaus, I.V. Krivosheina, A. Dietz, and O. Chkvorets, *Phys. Lett. B* **586**, 198 (2004); final data analysis reported in: H.V. Klapdor-Kleingrothaus and I.V. Krivosheina, *Mod. Phys. Lett. A* **21**, 1547 (2006).
 - [10] Review of Particle Properties, W.M. Yao *et al.*, *J. Phys. G* **33**, 1 (2006).
 - [11] N. Severijns, M. Beck, and O. Naviliat-Cuncic, *Rev. Mod. Phys.* **78**, 991 (2006).
 - [12] V.A. Rodin, A. Faessler, F. Šimkovic, and P. Vogel, *Nucl. Phys. A* **766**, 107 (2006); *Erratum* **793**, 213 (2007).
 - [13] M. Kortelainen, O. Civitarese, J. Suhonen, and J. Toivanen, *Phys. Lett. B* **647**, 128 (2007); M. Kortelainen and J. Suhonen, *Phys. Rev. C* **75**, 051303(R) (2007); *ibidem* **76**, 024315 (2007).
 - [14] E. Caurier, G. Martínez-Pinedo, F. Nowacki, A. Poves, and A.P. Zuker, *Rev. Mod. Phys.* **77**, 427 (2005).
 - [15] V. Rodin and A. Faessler, arXiv:0707.2742 [nucl-th].
 - [16] F. Osterfeld, *Rev. Mod. Phys.* **64**, 491 (1992).
 - [17] A. Bohr and B.R. Mottelson, *Phys. Lett. B* **100**, 10 (1981).
 - [18] G.F. Bertsch and I. Hamamoto, *Phys. Rev. C* **26**, 1323 (1982).
 - [19] S.R. Elliott and J. Engel, *J. Phys. G* **30**, R183 (2004).
 - [20] H. Ejiri, *Phys. Rep.* **338**, 265 (2000).
 - [21] V.I. Tretyak and Y.G. Zdesenko, *Atomic Data and Nuclear Data Tables* **80**, 83-116 (2002).
 - [22] S. Stoica and H.V. Klapdor-Kleingrothaus, *Phys. Rev. C* **63**, 064304 (2001).
 - [23] D. Cha, *Phys. Rev. C* **27**, 2269 (1983).
 - [24] P. Vogel and M.R. Zirnbauer, *Phys. Rev. Lett.* **57**, 3148 (1986); J. Engel, P. Vogel, and M.R. Zirnbauer, *Phys. Rev. C* **37**, 731 (1998).
 - [25] F. Šimkovic, A. Faessler, V.A. Rodin, P. Vogel, and J. Engel, arXiv:0710.2055 [nucl-th].
 - [26] K. Zuber, Consensus Report of the Workshop on “Matrix Elements for Neutrinoless Double Beta Decay” (Durham, UK, 2005) [arXiv:nucl-ex/0511009].
 - [27] C. Volpe, *J. Phys. G* **31**, 903 (2005).
 - [28] O. Civitarese and J. Suhonen, *Nucl. Phys. A* **761**, 313 (2005).
 - [29] J. Suhonen, in the Proceedings of *INPC'04*, 22nd Intern. Nuclear Physics Conference (Göteborg, Sweden, 2004), ed. by B. Jonson, M. Meister, G. Nyman, and M. Zhukov, *Nucl. Phys. B* **752**, 53c (2005).
 - [30] J. Suhonen, *Phys. Lett. B* **607**, 87 (2005).
 - [31] M. Kortelainen and J. Suhonen, *Europhys. Lett.* **58**, 666 (2002); J. Suhonen and M. Kortelainen, in the Proceedings of *MEDEX'05* [32], p. 519.
 - [32] A.S. Barabash, Proceedings of *MEDEX'05*, 5th Int. Workshop on Matrix Elements for the Double-beta Decay Experiments, edited by I. Stekl and O. Civitarese, *Czech. J. Phys.* **56**, 437 (2006); A.S. Barabash, Proceedings of *Neutrino 2006*, 2nd International Conference on Neutrino Physics and Astrophysics (Santa Fe, New Mexico, 2006) [arXiv:hep-ex/0608054], to appear.
 - [33] A. García *et al.*, *Phys. Rev. C* **47**, 2910 (1993).
 - [34] J.F. Wilkerson, “Electron Capture Branch of ^{100}Tc ,” electronic Proceedings of *NNR'05*, Workshop on Neutrino Nuclear in Double Beta Decays and Low-energy Astro-neutrinos (Osaka, Japan, 2005), www.spring8.or.jp/ext/en/appeal/nnr05
 - [35] M. Bhattacharya *et al.*, *Phys. Rev. C* **58**, 1247 (1998).
 - [36] Evaluated Nuclear Structure Data File, www.nndc.bnl.gov/ensdf
 - [37] H. Akimune *et al.*, *Phys. Lett. B* **394**, 23 (1997).
 - [38] R. Madey *et al.*, *Phys. Rev. C* **40**, 540 (1989).
 - [39] M. Sasano *et al.*, in the Proceedings of *COMEX 2*, 2nd Int. Conf. on Collective Motion in Nuclei under Extreme Conditions (Sankt Goar, Germany, 2006), ed. by P. von Neumann-Cosel and T. Aumann, *Nucl. Phys. A* **788**, 76c (2007).
 - [40] S. Rakers *et al.*, *Phys. Rev. C* **71**, 054313 (2005).
 - [41] T. Suzuki, D.F. Measday, and J.P. Roalsvig, *Phys. Rev. C* **35**, 2212 (1987).
 - [42] D. Frekers, J. Dilling, and I. Tanihata, *Can. J. Phys.* **99**, 1 (2006); available at titan.triumf.ca/research/EC.shtml
 - [43] D. Frekers, talk at *MEDEX'07*, 6th Int. Workshop on Matrix Elements for the Double-beta Decay Experiments (Prague, Czech Rep., 2007), available at medex07.utef.cvut.cz
 - [44] D.R. Zinatulina and A. Klinskikh, talks at *MEDEX'07* [43].
 - [45] N.T. Zinner, K. Langanke, and P. Vogel, *Phys. Rev. C* **74**, 024326 (2006).
 - [46] R.G.T. Zegers *et al.*, *Phys. Rev. C* **74**, 024309 (2006); R.G.T. Zegers *et al.*, arXiv:0707.2840 [nucl-ex].

- [47] K. Amos, A. Faessler, and V. Rodin, Phys. Rev. C **76**, 014604 (2007).
- [48] A. Griffiths and P. Vogel, Phys. Rev. C **46**, 181 (1992).
- [49] V.A. Rodin, A. Faessler, F. Šimkovic, and P. Vogel, Phys. Rev. C **68**, 044302 (2003).
- [50] S. Singh, R. Chandra, P.K. Rath, P.K. Raina, and J.G. Hirsch, Eur. Phys. J. A **33**, 375 (2007).
- [51] R. Alvarez-Rodriguez, P. Sarriguren, E. Moya de Guerra, L. Pacearescu, A. Faessler, and F. Šimkovic, Phys. Rev. C **70**, 064309 (2004).
- [52] F. Šimkovic, L. Pacearescu, and A. Faessler, Nucl. Phys. A **733**, 321 (2004).
- [53] G.A. Miller and J.E. Spencer, Ann. Phys. **100**, 562 (1976).
- [54] S. Raman, C.H. Malarkey, W.T. Milner, C.W. Nestor, Jr., and P.H. Stelson, Atomic Data and Nuclear Data Tables **36**, 1 (1987).

$2\nu 2\beta$ matrix elements

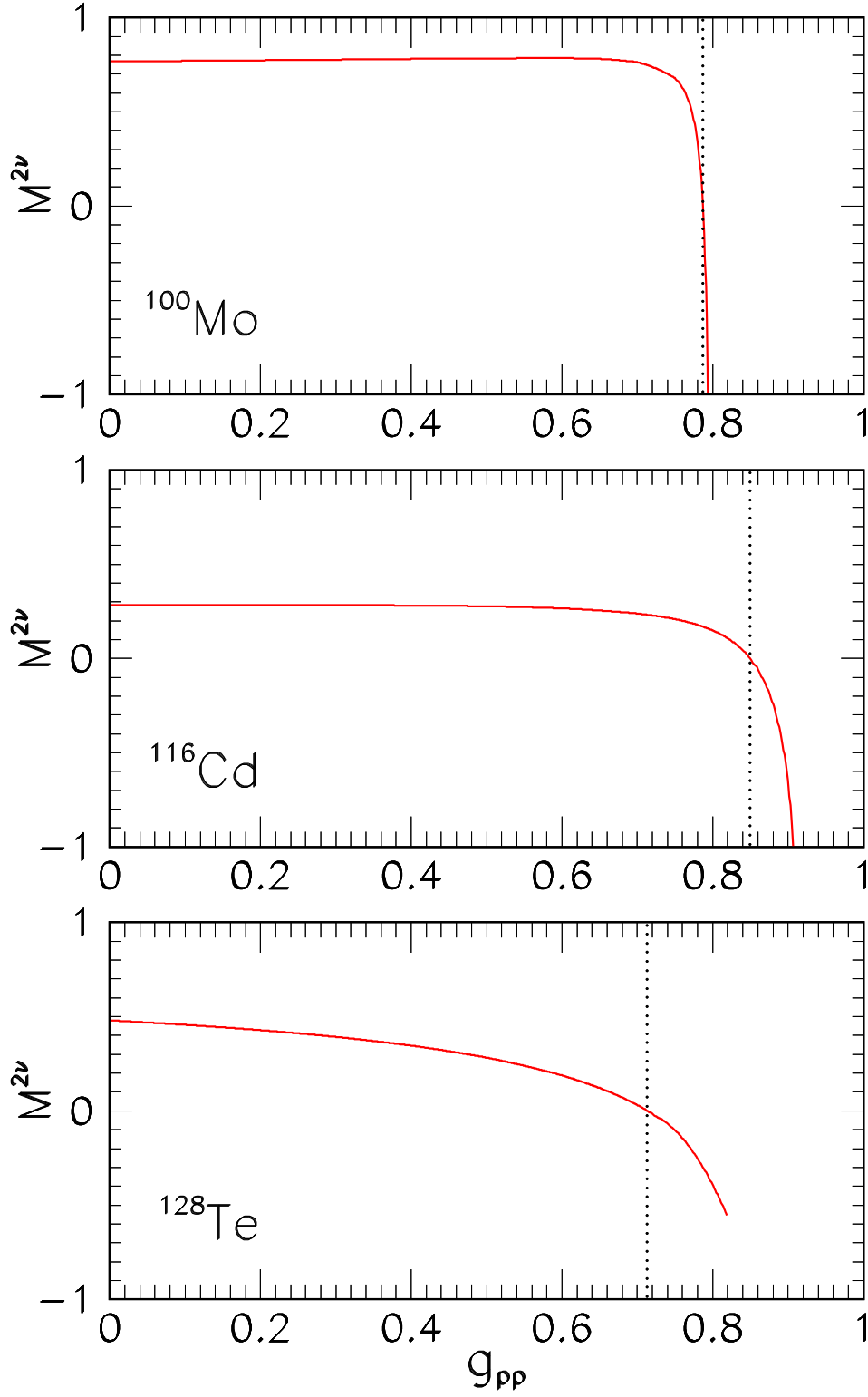


FIG. 1: Matrix elements for $2\nu 2\beta$ decay in QRPA (solid curves) as a function of g_{pp} , for ^{100}Mo , ^{116}Cd , and ^{128}Te . In each panel, the vertical dotted line marks the critical g_{pp} value where $M_{2\nu} = 0$. Calculations refer to large basis.

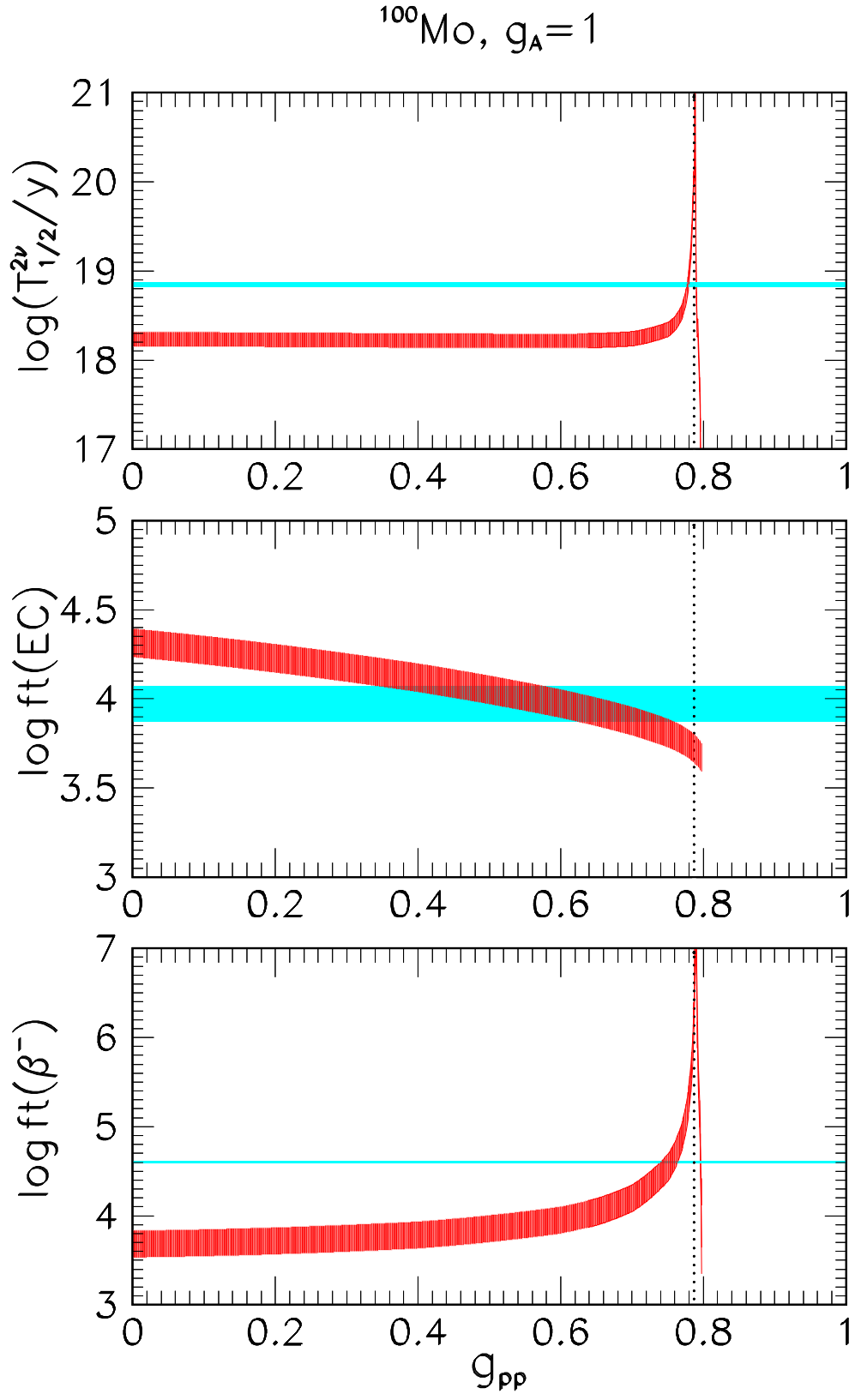


FIG. 2: Lifetimes for $2\nu 2\beta$, EC, and β^- decay in ^{100}Mo . Horizontal bands: experimental data. Curved bands: QRPA results as a function of g_{pp} , for fixed $g_A = 1$, in large basis. The vertical width of the bands corresponds to $\pm 1\sigma$ uncertainties.

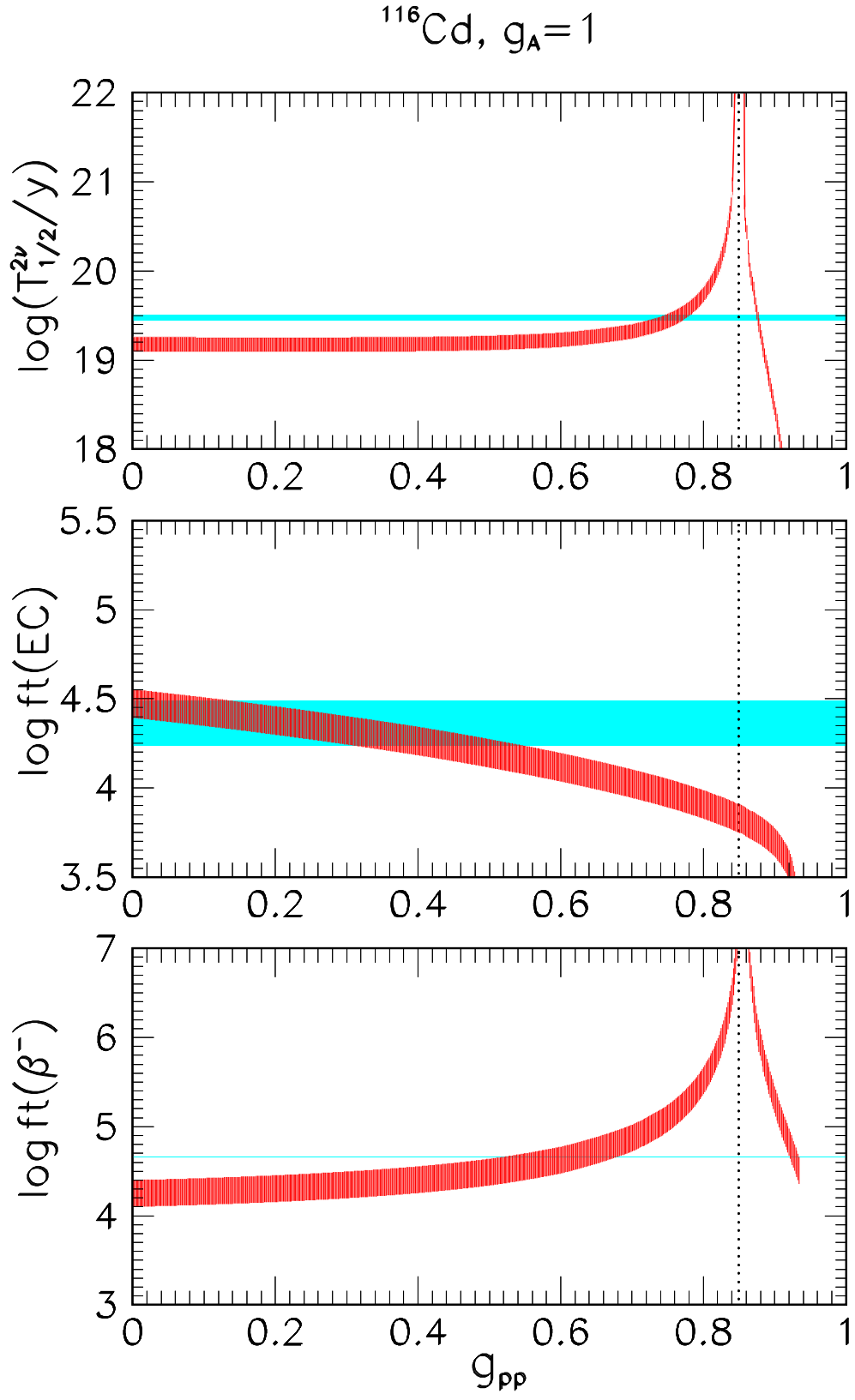


FIG. 3: Lifetimes for $2\nu 2\beta$, EC, and β^- decay in ^{116}Cd . Horizontal bands: experimental data. Curved bands: QRPA results as a function of g_{pp} , for fixed $g_A = 1$, in large basis. The vertical width of the bands corresponds to $\pm 1\sigma$ uncertainties.

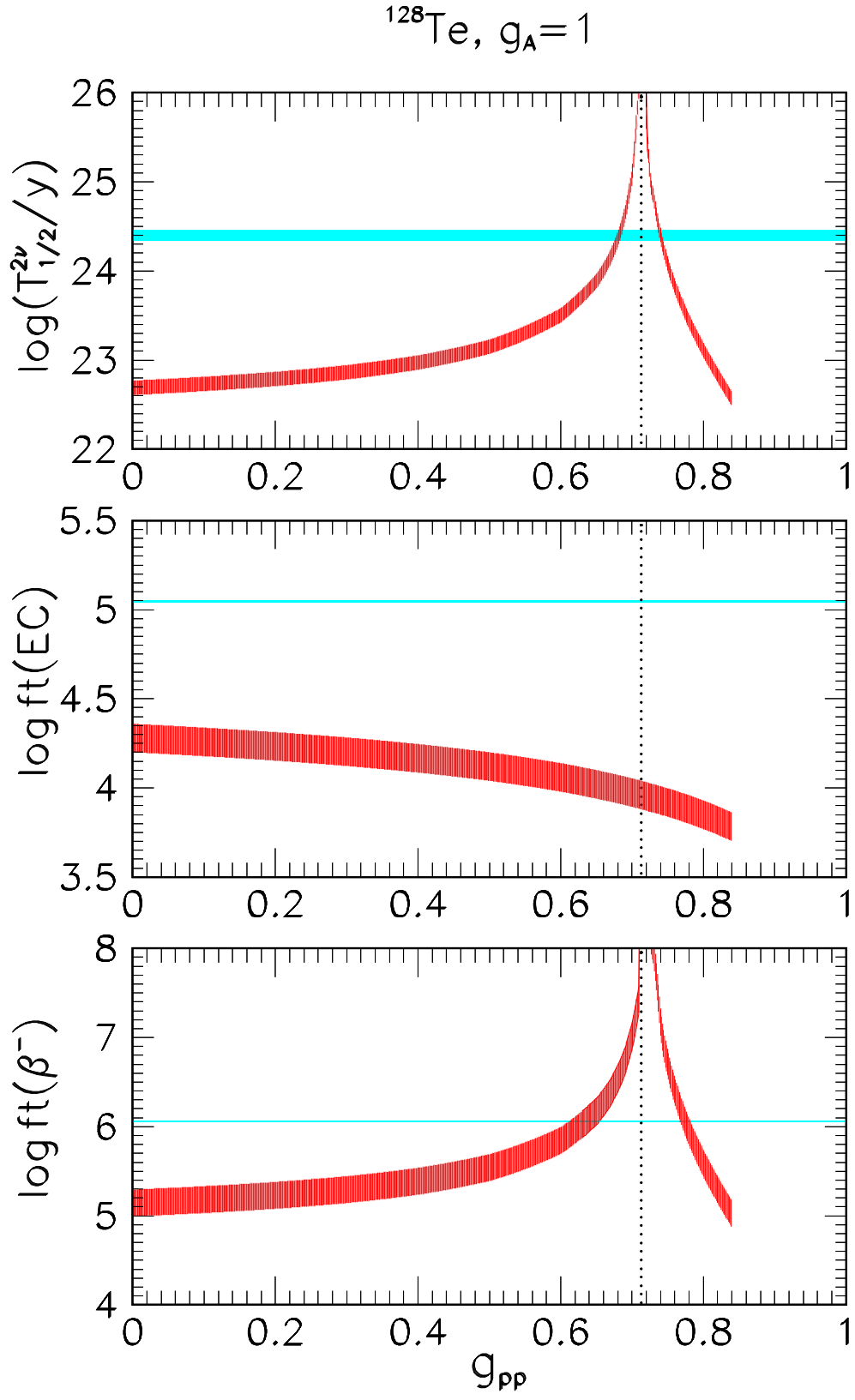


FIG. 4: Lifetimes for $2\nu 2\beta$, EC, and β^- decay in ^{128}Te . Horizontal bands: experimental data. Curved bands: QRPA results as a function of g_{pp} , for fixed $g_A = 1$, in large basis. The vertical width of the bands corresponds to $\pm 1\sigma$ uncertainties.

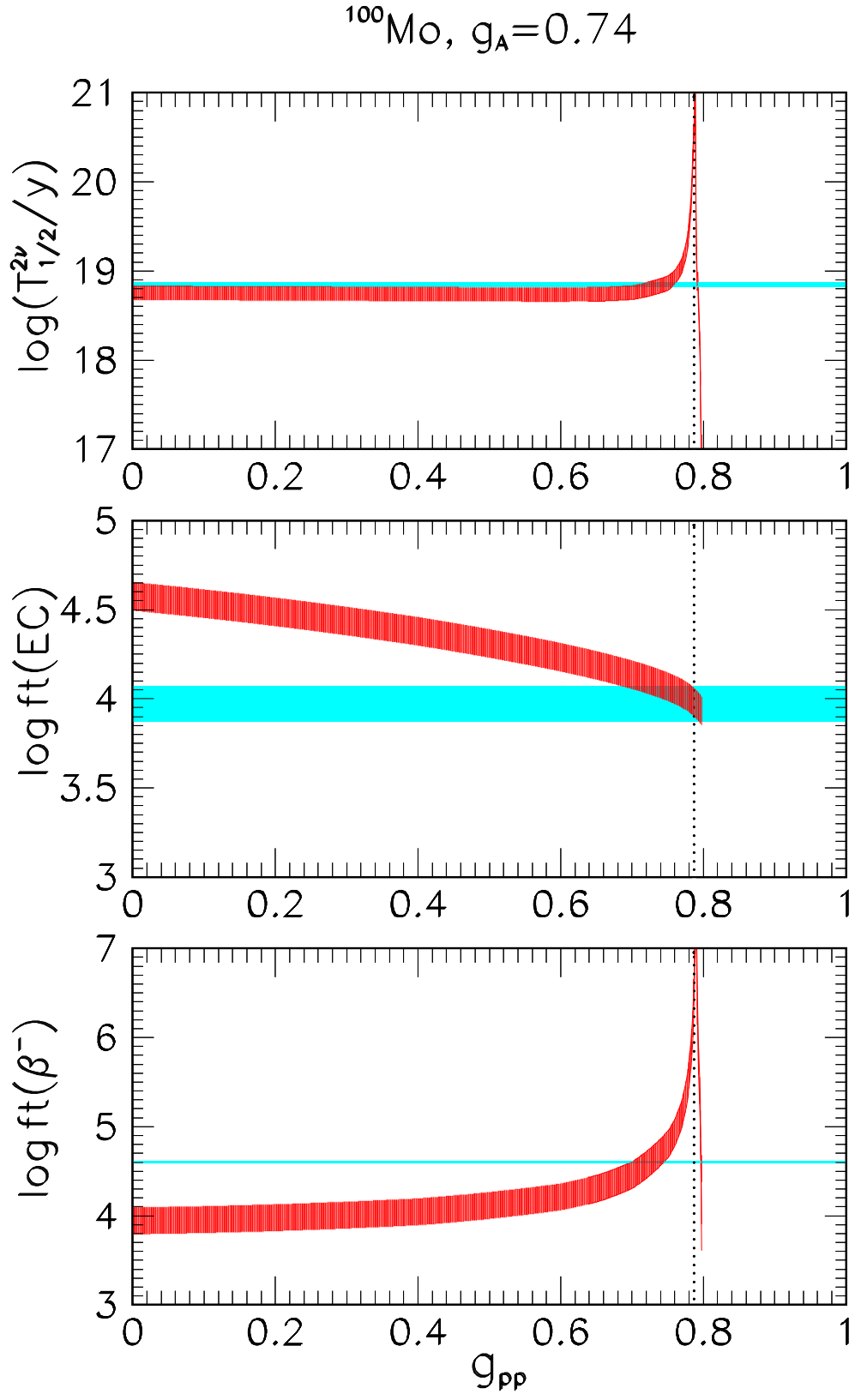


FIG. 5: As in Fig. 2, but for $g_A = 0.74$. Note the overall agreement of QRPA results with data for $g_{pp} \sim 0.73$.

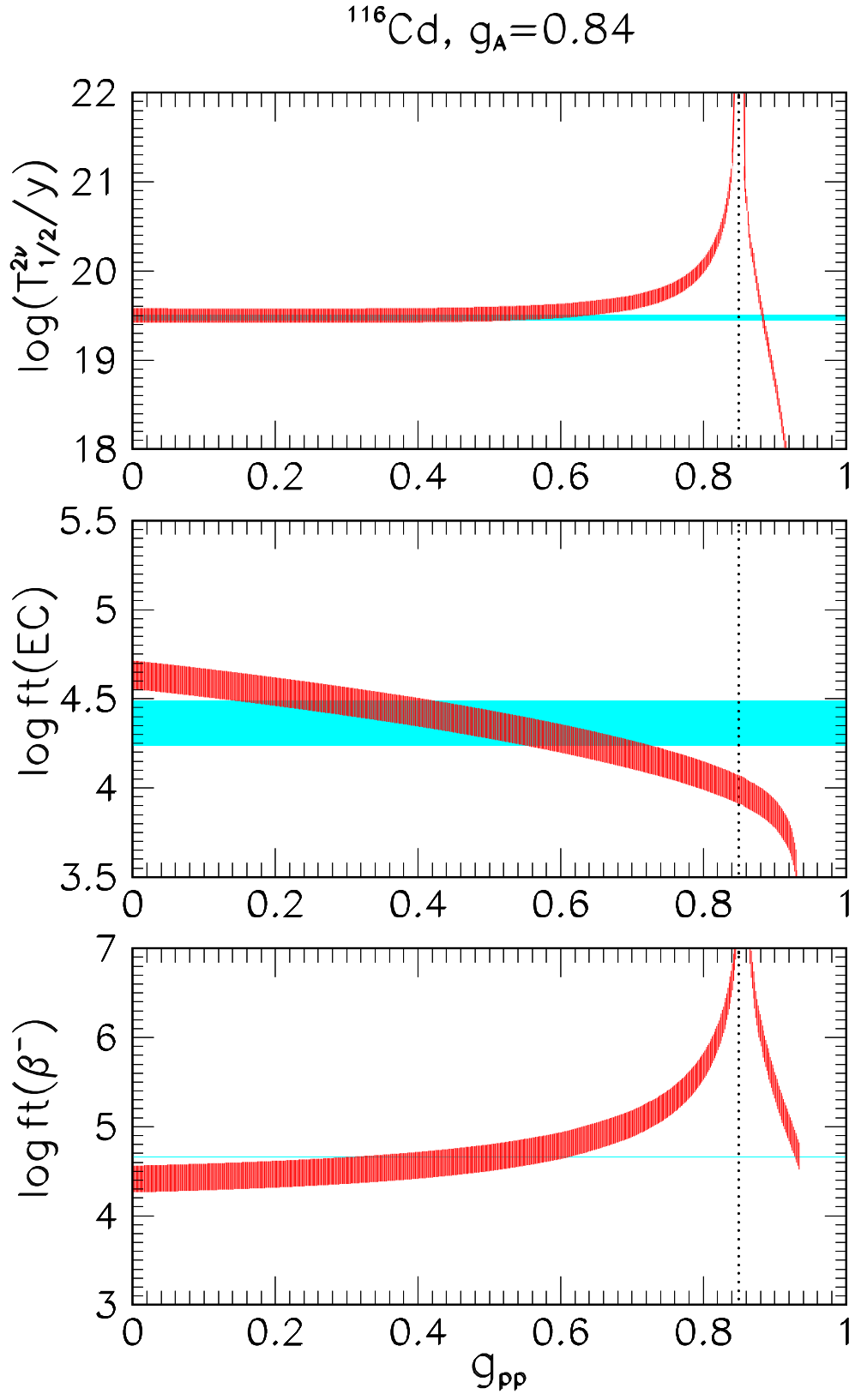


FIG. 6: As in Fig. 3, but for $g_A = 0.84$. Note the overall agreement of QRPA results with data for $g_{pp} \sim 0.5$.

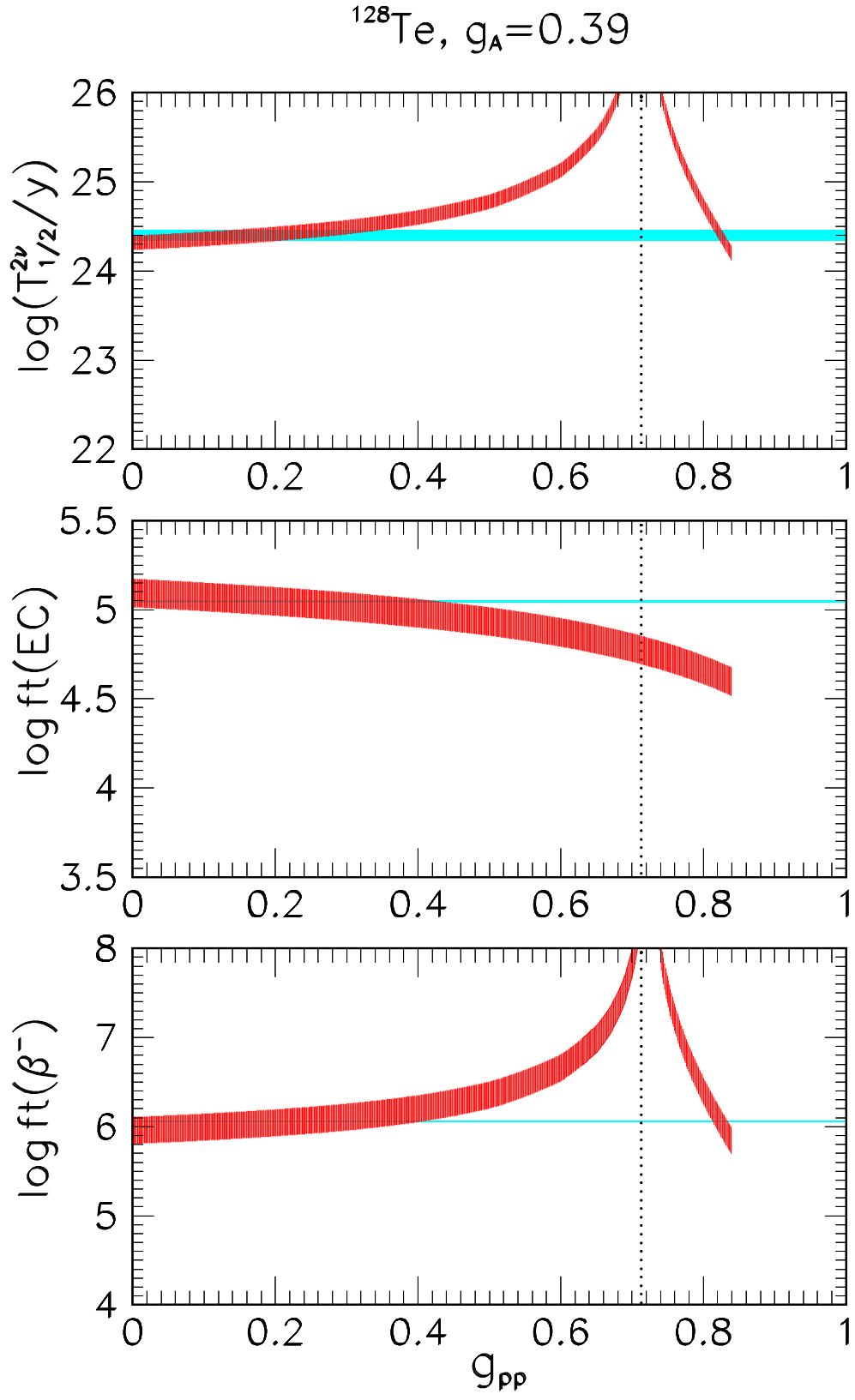


FIG. 7: As in Fig. 4, but for $g_A = 0.39$. Note the overall agreement of QRPA results with data for $g_{pp} \sim 0.2$.

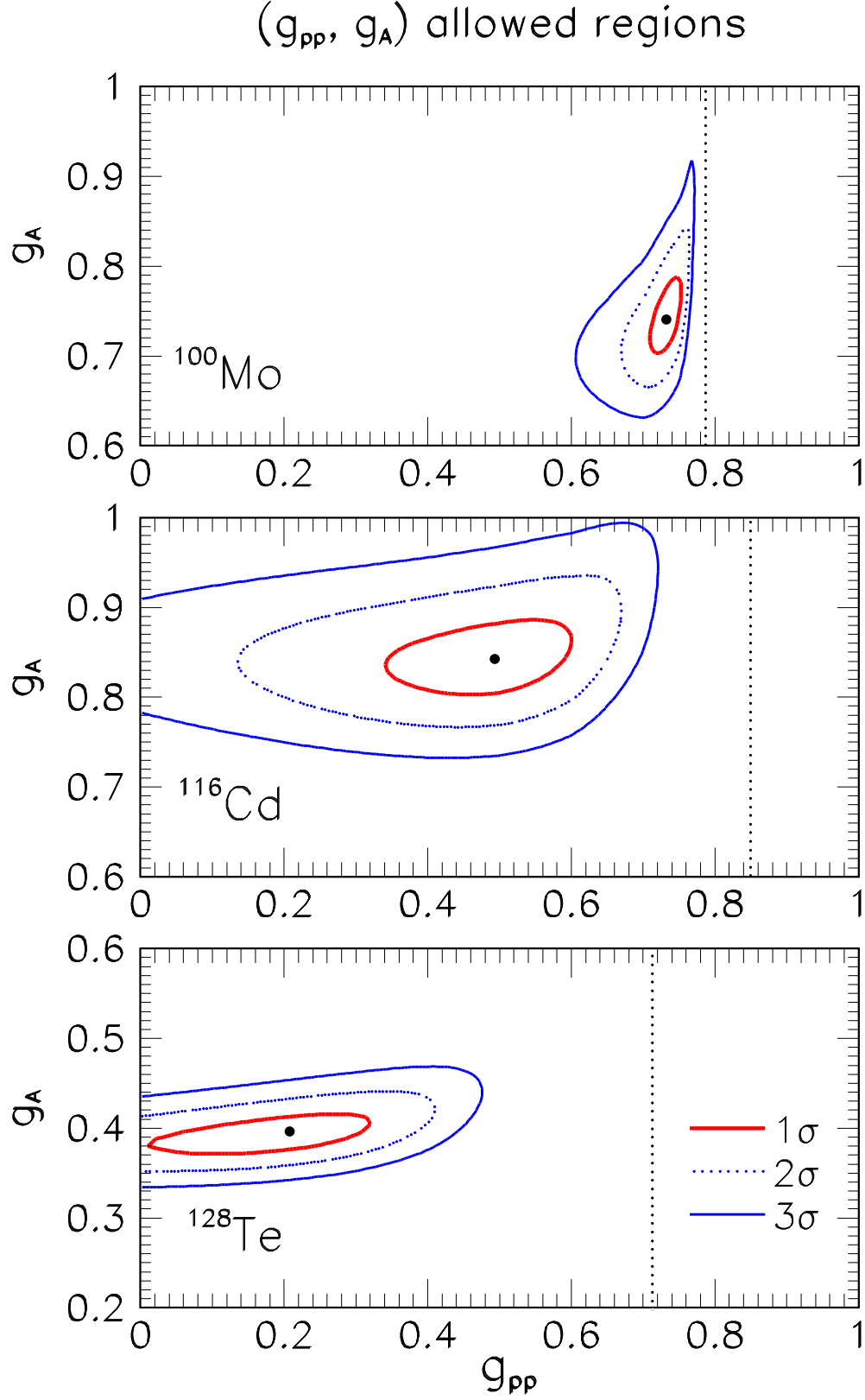


FIG. 8: Regions allowed at $n\text{-}\sigma$ in the (g_{pp}, g_A) plane from a QRPA fit to $2\nu 2\beta$, EC, and β^- data, in each of the three nuclei ^{100}Mo , ^{116}Cd , and ^{128}Te . QRPA calculations refer to large basis.

$0\nu 2\beta$ matrix element components

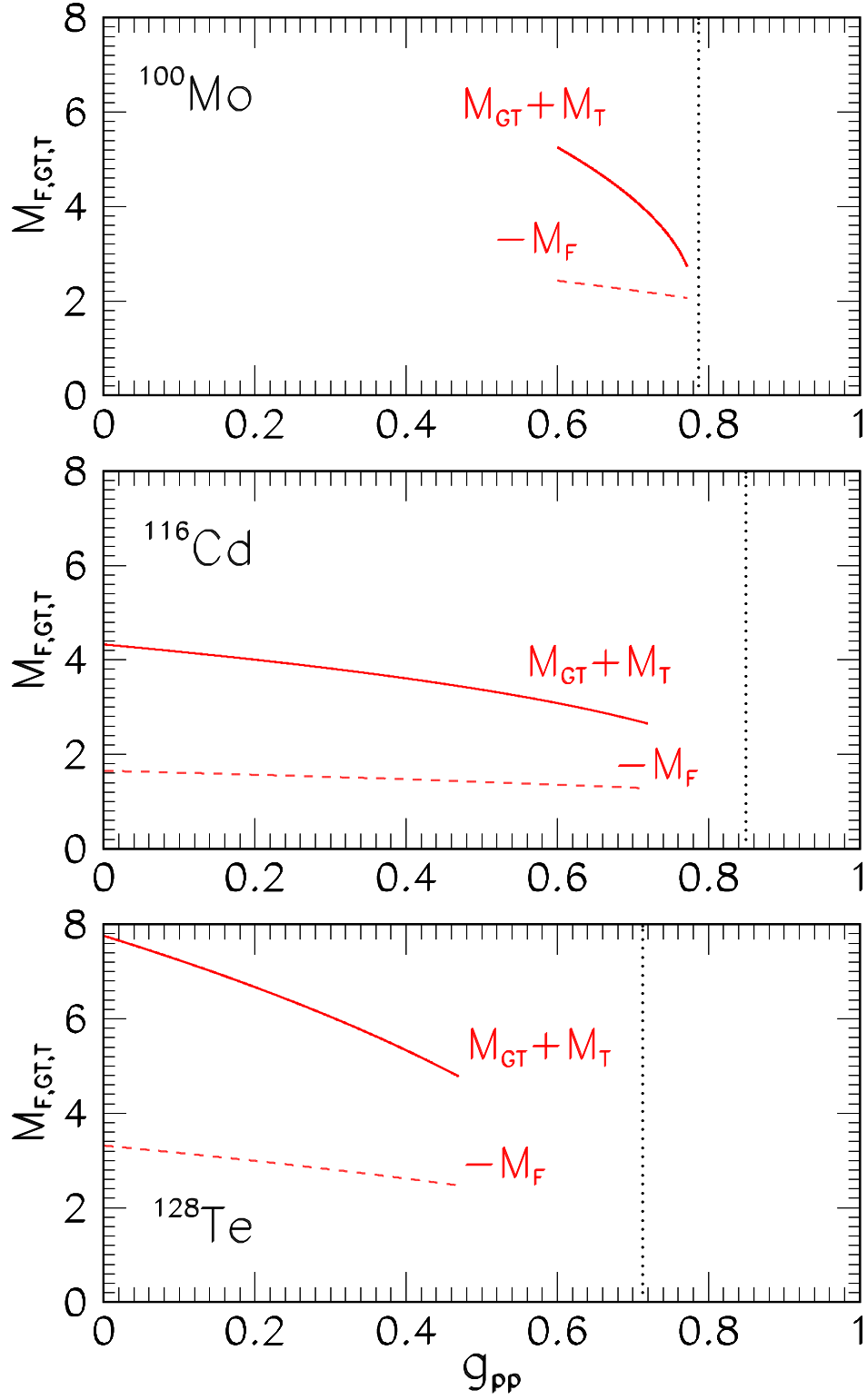


FIG. 9: $0\nu 2\beta$ matrix element components $M_{GT}^{0\nu} + M_T^{0\nu}$ (solid) and $-M_F^{0\nu}$ (dashed), as a function of the g_{pp} parameter in its 3σ allowed range (see Fig. 8). QRPA calculations refer to the default case (large basis with short range correlations).

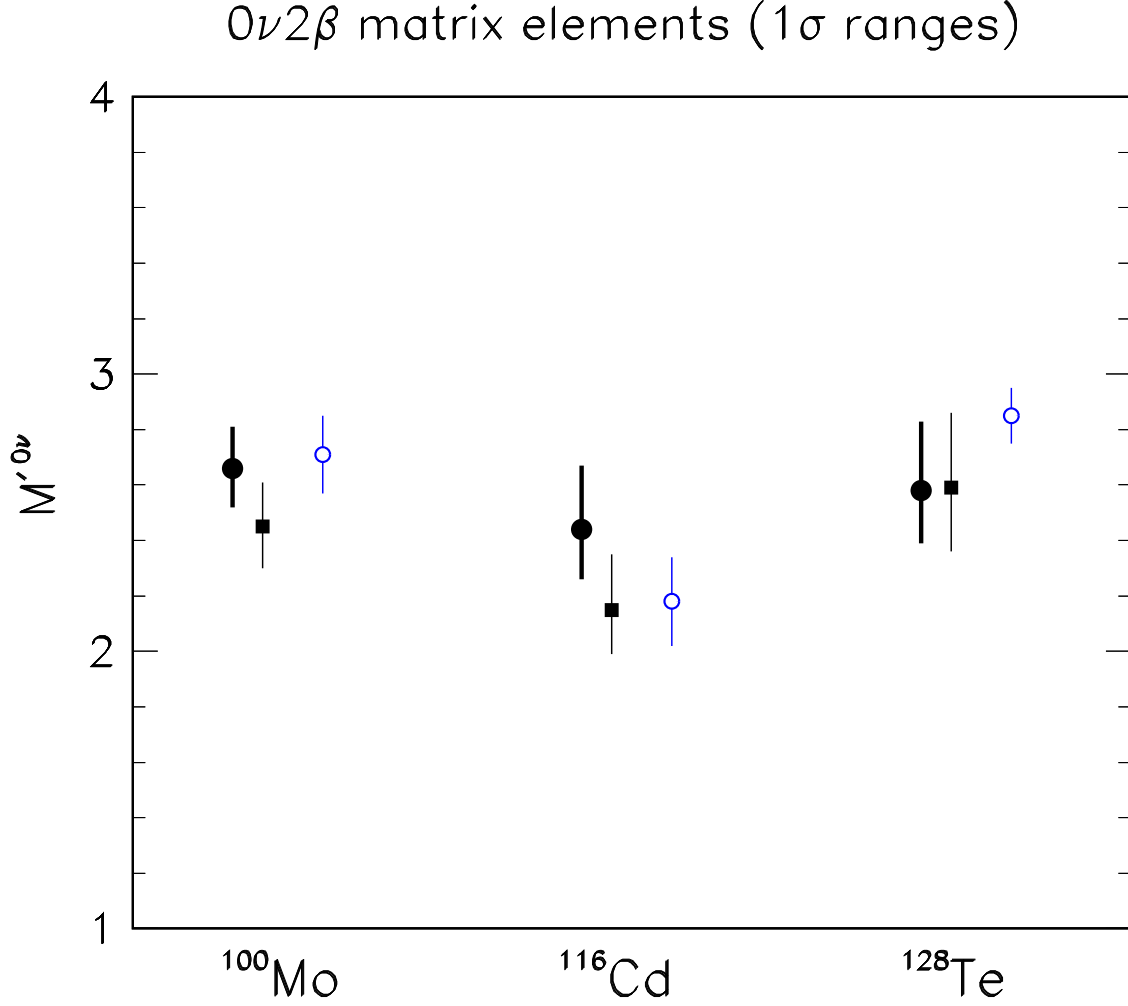


FIG. 10: Overview of $0\nu 2\beta$ matrix elements $M'^{0\nu}$, together with their $\pm 1\sigma$ estimated errors. For each nucleus, three QRPA cases are shown. From the left to right, the first two cases correspond to the results of this work in large basis (black circle, with thick error bars) and in small basis (black square). The error bars for these two cases encompass the uncertainties in both parameters (g_{pp} , g_A) from the fit to ($2\nu 2\beta$, EC, β^-) data. The third case (white circle) refers to the previous results of Ref. [12], as obtained for the fixed value $g_A = 1$ (with g_{pp} adjusted to $2\nu 2\beta$ data). All cases include Jastrow-like s.r.c. effects.